

5. CALCAREOUS NANNOFOSSIL BIOSTRATIGRAPHY FROM A 15-KM TRANSECT (COCOS PLATE TO CARIBBEAN PLATE) ACROSS THE MIDDLE AMERICA TRENCH, NICoya PENINSULA, COSTA RICA¹

Jay P. Muza²

ABSTRACT

Three Pleistocene, five Pliocene, and thirteen late and middle Miocene calcareous nannofossil datums have been identified in the Leg 170 cored sequences collected from a transect across the Middle America Trench off the Nicoya Peninsula. Although some nannofossil zones could not be delineated, particularly in the Pliocene and upper Miocene, there appears to be a complete or very nearly complete Pleistocene through lower Miocene section at Sites 1039 and 1040. The oldest assemblages, observed at Site 1039 and 1040, are latest early Miocene in age (nannofossil Zone NN4). These assemblages are associated with gabbro intrusions into the basal sediments (one contact metamorphic hornfels sample contains relict nannofossils), indicating an age for the intrusion event of between 15.6 and 18.2 Ma at both Sites 1039 and 1040. Reference Site 1039, located on the Cocos plate, provides the best-preserved sequence of sediments of late Pleistocene to latest early Miocene age. The sediments cored in the prism sections at Sites 1040, 1041, 1042, and 1043 all indicate that the age of nannofossil assemblages in the prism sediments, including the toe, wedge, and apron, are all Pleistocene with a considerable amount of upper Miocene reworking.

A period of low sediment accumulation rates (~5.3 m/m.y.) is recorded for Pliocene and upper Miocene sediments at Sites 1039, 1040,

¹Muza, J.P., 2000. Calcareous nannofossil biostratigraphy from a 15-km transect (Cocos plate to Caribbean plate) across the Middle America Trench, Nicoya Peninsula, Costa Rica. In Silver, E.A., Kimura, G., and Shipley, T.H. (Eds.), *Proc. ODP, Sci. Results*, 170, 1–63 [Online]. Available from World Wide Web: <http://www-odp.tamu.edu/publications/170_SR/VOLUME/CHAPTERS/SR170_05.PDF>. [Cited YYYY-MM-DD]

²Department of Physical Sciences (Oceanography), Broward Community College Central Campus, Davie FL 33314, USA. jmuza@broward.cc.fl.us

and 1043. Pliocene calcareous nannofossil assemblages characteristic of the ~2.5- to 3.75-m.y. time interval (nannofossil Zones NN16 and equivalent nannofossil Subzones CN12b and CN12a) were not resolved at any site. Nannofossil Zones NN15, NN14, NN13, and NN12 (early late Pliocene to early Pliocene) could not be resolved at any site either because of the absence of marker species. Within the Miocene at Sites 1039 and 1040, nannofossil Zones NN10–NN6 were difficult to differentiate because of the absence of several species that define the zonal boundaries. These intervals, where the nannofossil zones have not been resolved or are partially resolved, are primarily composed of carbonate ooze deposited during an ~8.5-m.y. (2.5–11 Ma) low sediment accumulation rate time interval. The absence of many of the marker species is attributed to warmer water conditions during those periods. Many of the same marker species are absent in the sediments recovered from nearby Deep Sea Drilling Project Site 155 in the Panama Basin.

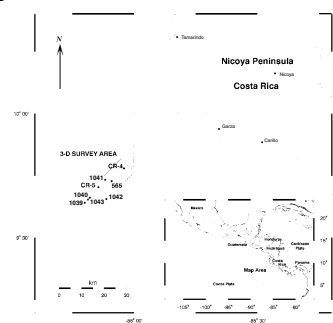
INTRODUCTION

Subduction of oceanic lithosphere, with its blanket of biogenous and terrigenous sediments, is an essential part of the global pathway by which the solid earth is recycled. This part of the cycle is also the least documented and, therefore, the least understood, in terms of the mass balance between subducting oceanic lithosphere, the portion of the lithosphere that descends into the mantle, and the portion that emerges elsewhere (Kimura, Silver, Blum, et al., 1997). Part of the subducted lithosphere may be accreted to or may underplate the overriding plate, released through pore water kinetics and chemistry and ultimately ejected or released as volcanic solids, liquids, and gases or emplaced as magma plutons. An understanding of the nature of this recycling—particularly the amounts and rates at which the lithosphere is underplated or accreted—is important to understanding the processes of earthquake generation at subduction zones (Kimura, Silver, Blum, et al., 1997). In addition, determining the mass balance of carbonate material that enters the subduction zone and leaves as carbon dioxide and other carbon compounds is important in aiding our understanding of the complex cycle of carbon dioxide in our atmosphere, biosphere, and lithosphere and the impacts to trends in global temperatures. To this end, Ocean Drilling Program (ODP) Leg 170 drilled and cored oceanic lithosphere in a transect across the Middle America Trench, off of the Nicoya Peninsula, Costa Rica (Fig. F1). A comprehensive investigation has been undertaken to arrive at an understanding of the fate of subducted materials. One study of importance to this endeavor is the derivation of accurately age-dated fossils from the Leg 170 cores.

PURPOSE

The purpose of this study is to synthesize and provide as accurate and precise age-depth models as possible, utilizing calcareous nannofossils for age determination, for all of the cores recovered during ODP Leg 170 seaward of the Costa Rican Nicoya Peninsula on the subducted margin. Comprehensive calcareous nannofossil species range and distribution charts have been constructed from all the sites cored during Leg 170 from which the age-depth models have been synthesized.

F1. Location of Leg 170 Sites 1039, 1040, 1041, 1042, and 1043 offshore of the Nicoya Peninsula, p. 23.



The primary focus of Leg 170 was to core a series of sites off of the Costa Rican Nicoya Peninsula in an effort to understand what happens to the pelagic and hemipelagic sediments, associated pore waters, and oceanic basement that enter the subduction zone off the Costa Rican margin (Kimura, Silver, Blum, et al., 1997). The Costa Rica subduction margin was chosen because the volume of incoming sediments into the trench is thought to have been relatively constant over long periods of time and the influx of turbidites into the trench system appears to have been minimal.

Five sites were drilled during Leg 170 perpendicular to and across the Middle America Trench along a 15-km transect (Figs. F1, F2). Site 1039 was drilled seaward of the trench on the Cocos plate and acts as a reference for the age, thickness, lithology, physical properties, and fluid composition of the incoming sedimentary block into the trench. Site 1039 also reached basaltic crust.

Site 1040 (Figs. F1, F2) was drilled on the Caribbean plate immediately to the east of the Middle America Trench through the accretionary wedge, the décollement, and the underthrust sedimentary section to basement. This site was drilled to determine the age, the portion of the incoming section that is accreted, the physical and chemical properties, and the changes in chemistry and physical properties between the underthrust sedimentary and basaltic rocks and the reference section.

Site 1043 (Figs. F1, F2) was drilled with the same objectives as Site 1040 but was located closer to the trench axis, on the toe of the wedge, where the sediments overlying the décollement are not as thick.

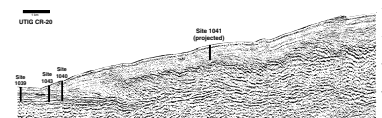
Sites 1041 and 1042 (Figs. F1, F3) were also drilled on the Caribbean plate with the purpose of penetrating through the slope apron into the underlying prism to determine the age and makeup of the apron and prism sediments.

A bathymetric map of the study area is provided (Fig. F4) in order to illustrate the location and depth of all five Leg 170 sites relative to each other.

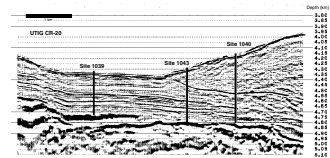
METHODS

Samples were processed to separate the clay-sized nannofossil fraction from the rest of the sediments by suspending the raw sediment in water then transferring the clay-sized portion to a coverslip using a pipette. The material on the coverslip was dried, then the coverslip was cemented to a glass microscope slide using Norland optical adhesive. Although this sample preparation technique is more time consuming than the standard smear-slide analyses done aboard ship for all of the core-catcher samples, it allows for better distribution of nannofossils on a microscope slide and a much higher confidence level of reproducibility in quantitative or semiquantitative analyses. All samples were processed this way except for the core-catcher samples and the relatively small numbers of smear-slide samples routinely prepared from split core surfaces during the Leg 170 cruise. In the latter case, raw sediment samples were mixed with enough water to form a thin, viscous slurry on a coverslip, then the slurry was allowed to dry before it was cemented to a glass slide with Norland optical adhesive. All samples were observed and analyzed using phase contrast and cross-polarized light under magnifications of 500 \times and 1250 \times . The diameter of the field of view at 1250 \times is ~0.16 mm.

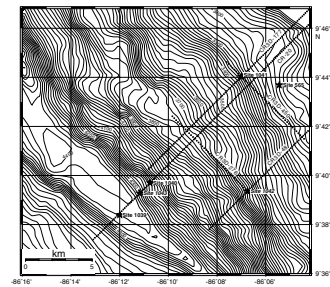
F2. Seismic reflection profile CR-20 showing the locations of Site 1039 reference section and Sites 1040 and 1043, p. 24.



F3. Seismic reflection profile CR-20 showing the projected location of Site 1041 relative to Sites 1039, 1040, and 1043, p. 25.



F4. Bathymetric map of the Leg 170 study area showing the depth and location of the five Leg 170 sites, p. 26.



Calcareous nannofossil range-distribution charts were constructed for all nannofossil species observed in each hole cored at Sites 1039, 1040, 1041, 1042, and 1043. The distribution, relative abundance, and relative preservation of nannofossil species observed in the cores at these sites are plotted on Tables **T1**, **T2**, **T3**, **T4**, **T5**, and **T6** along with the nannofossil zonation. Letters used to express species abundance are keyed to the \log_{10} of the number of specimens of a particular species or genus likely to be observed in any one field of view at a magnification of 1250 \times . The letters are denoted as follows:

- H = highly abundant (>100 specimens per field of view);
- V = very abundant (11–100 specimens per field of view);
- A = abundant (1–10 specimens per field of view);
- C = common (1 specimen per 2–10 fields of view);
- F = few (1 specimen per 11–100 fields of view); and
- R = rare (1 specimen per 101–1000 fields of view).

Through visual inspection at 1250 \times , a qualitative determination was made of the state of preservation of the nannofossils in each sample. In any given sample, the state of preservation may differ between each individual species, genus, or morphologic group. Thus, any qualitative measurement of a given sample must be based on the overall preservation qualities of the nannofossil assemblage. The following basic criteria were used to qualitatively describe the degree of preservation, dissolution, or overgrowth of a nannofossil assemblage:

- G = good (individual specimens exhibit no dissolution or overgrowth);
- M = moderate (individual specimens yield slight evidence of overgrowth or dissolution, central bars of gephyrocapsids are present, and elements of calcidiscids are prominent); and
- P = poor (individual specimens exhibit considerable dissolution and overgrowth, placoliths are ragged, gephyrocapsids commonly have their central bars dissolved, elements are not distinguishable in calcidiscids, and species identification is difficult).

Descriptions of species noted in this study and their references can be found in Perch-Nielsen (1985). A list of species noted in this study can be found in the “[Taxonomic Appendix](#),” p. 21.

STRATIGRAPHIC STANDARDS

Stratigraphic resolution and calcareous nannofossil age datums derived for the Leg 170 calcareous nannofossil record have been determined by applying the global calcareous nannofossil extinction event (last occurrence datum [LOD]), global appearance event (first occurrence datum [FOD]), and paleomagnetic datums as outlined in Berggren et al. (1995a, 1995b). In addition, the standard calcareous nannoplankton zones of Martini (1971), Bukry (1973b, 1975), and Okada and Bukry (1980) have been determined for the calcareous nannofossil distribution recorded from the Leg 170 cores (Tables **T1**, **T2**, **T3**, **T4**, **T5**, **T6**). The comprehensive correlation between the nannofossil zones of Martini (1971) and Bukry (1973b, 1975) used in this study and the astronomical/geomagnetically derived chronologic scale of Berggren et al.

T1. Calcareous nannofossil range-distribution chart and nannofossil zonation for Holes 1039A, 1039B, and 1039C, p. 34.

T2. Calcareous nannofossil range-distribution chart and nannofossil zonation for Hole 1040B, p. 44.

T3. Calcareous nannofossil range-distribution chart and nannofossil zonation for Hole 1040C, p. 46.

T4. Calcareous nannofossil range-distribution chart and nannofossil zonation for Holes 1041A, 1041B, and 1041C, p. 51.

T5. Calcareous nannofossil range-distribution chart and nannofossil zonation for Holes 1042A and 1042B, p. 56.

T6. Calcareous nannofossil range-distribution chart and nannofossil zonation for Hole 1043A, p. 57.

(1995a, 1995b) is shown in Figure F5 for the Pleistocene and Pliocene and Figure F6 for the Miocene.

In this study, the last observed occurrence of a particular species is called its top and the first observed occurrence of a particular species is called its bottom. Top and bottom are used because paleontologists generally work cores downsection, thus observing the top of a species range first and the bottom of the range farther down the core. In all of our cored intervals, it is unknown whether the actual first occurrence (new species introduction) or actual last occurrence (extinction) of an index fossil has been observed. Nevertheless, for the purposes of reporting an absolute date to a particular top or bottom, the LOD or FOD of the species will be reported. The ages of the bottom or top of the observed ranges of calcareous nannofossil species identified in this study are outlined in Table T7.

LEG 170 CALCAREOUS NANNOFOSSIL BIOSTRATIGRAPHIC SYNTHESIS

A synthesis of the occurrence of calcareous nannofossils recovered from the cored sequences at Sites 1039, 1040, 1041, 1042, and 1043 is presented. For each site, a composite section combining all of the holes cored has been constructed and the geologic framework for each site is characterized. Because the primary purpose of the nannofossil analyses at all the Leg 170 sites is to establish a geologic age-depth model for the sediments cored at each site, most of the nannofossil analyses centers on locating the top and bottom of the ranges of index nannofossil species in the cores and assigning nannofossil zones to the cored sequences. The zonation of Martini (1971) provides the nannofossil zonation framework for this study. Martini's zones are defined in Table T8 and are determined by the range of the first and/or last occurrences of the listed index species. Also defined in Table T8 is the widely used nannofossil zonation scheme of Bukry (1973b, 1975) and Okada and Bukry (1980), an alternative to Martini's zonation scheme that can easily be adapted to the Leg 170 nannofossil data.

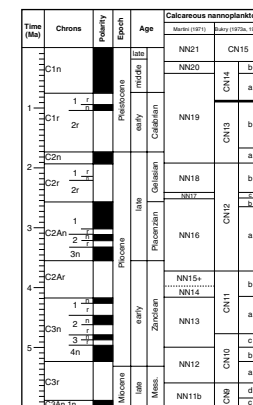
Site 1039

Three holes were cored at Site 1039 (located along seismic line CR-20) in a water depth of ~4352 m through the trench floor on the Cocos plate (Figs. F2, F4). Hole 1039A penetrated 28 meters below seafloor (mbsf) and recovered three cores. Hole 1039B penetrated 384.3 mbsf and recovered 42 cores. Hole 1039C was drilled to 363.1 mbsf and then cored to a depth of 448.7 mbsf; 11 cores were recovered. A composite diagram of total core recovery, depth cored, lithology, and age is provided in Figure F7. Core recovery from Holes 1039A and 1039B is near 100%, enhancing biostratigraphic resolution; core recovery from Hole 1039C is 44% primarily due to difficulties in drilling through 85 m of soft ooze, well-indurated breccia, and gabbro.

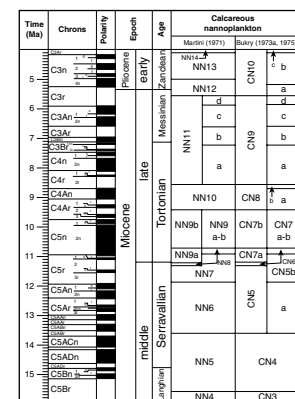
The upper 84 m (lithologic Unit U1) of sediment at Site 1039 is primarily a carbonate-poor diatom ooze (Fig. F7). In this section, calcareous nannofossils are present in only about one-third of the intervals sampled. The top 5.5 m of this section is comprised of turbidite.

A sharp decrease in both calcareous nannofossil and diatom abundances is observed between 84 and 133 mbsf (lithologic Unit U2). These

F5. Geologic time scale illustrating the comprehensive correlation between the nannofossil zones used in this study and the astronomical/geomagnetically derived chronologic scale for the Pleistocene and Pliocene, p. 27.



F6. Geologic time scale illustrating the comprehensive correlation between the nannofossil zones used in this study and the astronomical/geomagnetically derived chronologic scale for the Miocene, p. 28.



T7. Ages assigned to bottom and top of observed ranges of calcareous nannofossil species used for biostratigraphy, p. 60.

T8. Definition of calcareous nannofossil zonation scheme, p. 61.

sediments are silty clays near the top, but they become increasingly more calcareous downsection (133–152 mbsf) (Fig. F7). Pore-water geochemistry between 95 and 130 mbsf indicates low chloride concentrations (545 nM) corresponding to a 2% seawater dilution (Kimura, Silver, Blum, et al., 1997). According to Kimura, Silver, Blum, et al. (1997), this interval probably indicates a past low-chloride fluid conduit. Based on the diffusivity of chloride into the surrounding fluids, they suggest that this conduit existed prior to 180 ka. It is further suggested that the fluid flowing in this conduit prior to 180 ka affected the preservation of calcareous nannofossils and fossil diatoms. Nannofossil-size micrite is very abundant in the nannofossil-barren intervals between 95 and 130 mbsf and may represent diagenetically altered nannofossils. Subunit U2A (84.43–152.49 mbsf) contains <5% carbonate, whereas Subunit U2B has a fluctuating carbonate content of 5% to >20%. Subunit U2B represents a transitional zone from the hemipelagic sediments above to siliceous nannofossil ooze at 152 mbsf. Subunit U3A (152–180.38 mbsf) sediments are predominately siliceous nannofossil ooze with horizons of nannofossil-rich clay. Micrite is very common throughout these units, and carbonate content averages between 20% and 40%.

Subunit U3B (180.38–279.93 mbsf) consists of nannofossil ooze with >50% carbonate content. The change between Subunits U3A and U3B appears to be transitional until the abrupt disappearance of the clay layers at 180.38 mbsf. Nannofossils, diatoms, sponge spicules, foraminifers, radiolarians, and silicoflagellates (in order of decreasing abundance) make up the bulk of the sediment grains of Subunit U3B (Kimura, Silver, Blum, et al., 1997). Micrite is ubiquitous, and terrigenous grains of quartz and feldspar are absent or sporadically present in only trace amounts.

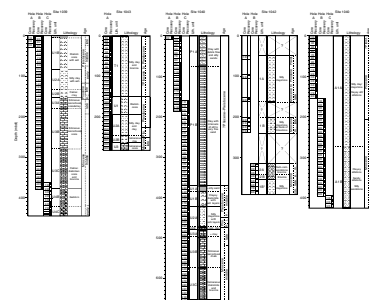
The siliceous component increases in proportion to the carbonate component beginning at 280 mbsf with the introduction of thin layers of diatom oozes consisting of mats of a single species of diatom *Thalassiothrix longissima*. Similar mats were observed during Leg 138 directly west of Site 139 in the eastern equatorial Pacific (Kimura, Silver, Blum, et al., 1997). Another characteristic of this lithology is the presence of coarse-grained matrix-supported breccias with clasts of carbonate and siliceous ooze. Analysis of the nannofossil assemblage of one of these clasts points to a late Miocene age for the assemblage. Subunit U3C extends to 378 mbsf.

Gabbro (basement?) was first encountered at 379 mbsf in Hole 1039B and at 422 mbsf in Hole 1039C (lithologic Unit U4). Mineralogically, samples from both sites seem to indicate the same intrusion (Kimura, Silver, Blum, et al., 1997). If the gabbro represents true basement rock, then the constrained age of the basement at this site is some 8 to 9 m.y. younger than previously thought. This will be discussed in detail in the next section.

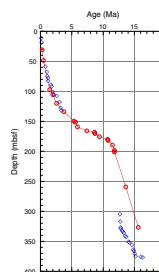
Nannofossil Distribution, Abundance, Preservation, and Chronology in Site 1039 Composite Section

The distribution, abundance, and preservation of calcareous nannofossils recovered from Holes 1039A, 1039B, and 1039C correlated to the nannofossil zonation scheme of Martini (1971) are presented in Table T1. An age-depth diagram plotting the age of all observed nannofossil datums at Site 1039 with the depth of observation is presented in Figure F8. The shipboard-derived paleomagnetic dates plotted in Figure F8 strongly match the age-depth relationships of the calcareous nannofos-

F7. Stratigraphic profile of composite lithologic sections from Sites 1039, 1043, 1040, 1042, and 1041, p. 29.



F8. Age-depth relationship of calcareous nannofossil datums from the composite section of Holes 1039B and 1039C, p. 31.



sil datums in the Pleistocene and Pliocene intervals. However, within the lower Miocene, there is clearly an abnormality in the paleomagnetic data, which indicates sediment accumulation rates much higher than normally expected for pelagic sediments.

0–84 mbsf (*Lithologic Units U1 and U2*)

In the top 84 m of the Site 1039 composite section, calcareous nannofossil preservation is poor to moderate and species occur very sporadically with depth (Table T1). Nannofossil Zones NN21 and NN20 are observed. The bottom of *Emiliania huxleyi* occurs at a depth of 31.03 mbsf and represents an age of 260 ka (Berggren et al., 1995b). The top of *Pseudoemiliania lacunosa* occurs at a depth of 48.75 mbsf and represents an age of 460 ka. The error associated with this depth, regarding the actual top of *P. lacunosa* at this site, is –3 m because of barren intervals immediately upsection.

84–140 mbsf (*Lithologic Unit U2*)

Nannofossils are essentially barren in samples taken between 84 and 120 mbsf (Table T1). As discussed earlier, the possibility of a fluid conduit between 95 and 130 mbsf before 180 ka may have contributed to the poor preservation of calcareous nannofossils in that interval. Within this section, however, are three locations that do contain nannofossils in sufficient quantity for biostratigraphy. One sample at 113 mbsf contains abundant nannofossils, albeit low in diversity, associated with micrite and with some evidence of etching. Another at 105 mbsf contains few poorly preserved species and associated micrite, and a third sample, at 97.37 mbsf, has common species abundances with moderate preservation and micrite. These samples have provided sufficient amounts of nannofossils to delineate two tops, *Helicosphaera sellii* at 97.37 mbsf and *Discoaster brouwerii* at 105.5 mbsf. The LOD of *H. sellii* is 1.47 Ma; the LOD of *D. brouwerii* is 1.95 Ma. The LOD of *D. brouwerii* to the LOD of *P. lacunosa* defines nannofossil Zone NN19.

The top of *Discoaster pentaradiatus* at 120.37 mbsf, corresponding to an LOD of 2.55 Ma, is found at the top of a 7-m sequence of abundant moderately to well-preserved nannofossils but still within the section represented by generally poor preservation or barren intervals due to the possible low-chloride pore-water conduit. The locations of the tops of *H. sellii*, *D. brouwerii*, and *D. pentaradiatus* in the cores (see Table T1) seem to indicate that their actual tops possibly may have been several meters upsection had the overlying intervals not been barren. However, when plotted against the paleomagnetic record for Site 1039, the top of each of these species integrates nicely with the paleomagnetic record (Fig. F8). Thus, the tops of these three species appear to represent highly reliable datums. The top of *D. pentaradiatus* to the top of *D. brouwerii* defines nannofossil Zone NN18. The tops of *Reticulofenestra pseudoumbilica* and *Sphenolithus* species are found at 134.21 mbsf. Both have a LOD of 3.75 Ma. Their tops in this core are considered to be reliable also.

Missing at Site 1039, between the tops of *D. pentaradiatus* and *R. pseudoumbilica*, are the tops of *D. surculus* (LOD = 2.55–2.59 Ma) and *D. tamalis* (2.73–2.78 Ma) (Table T1). Because these datums are not observed at Site 1039, the calcareous nannofossil zones defined by these datums (Zones NN17 and NN16 of Martini [1971] and Subzones CN12a, CN12b, and CN12c [Bukry, 1973a, 1973b]) cannot be resolved. However, the age-depth diagram for Site 1039 (Fig. F8) does not seem to indicate any breaks in the sediment age-depth record. Even more inter-

esting, these two datums are not observed at any of the other sites cored during Leg 170 (see “Site 1040,” p. 9, and “Site 1043,” p. 15). Evidence for a hiatus at these intervals is not supported by the Site 1039 age-depth curve (Fig. F8). It is possible then that both *D. surculus* and *D. tamalis* simply were not present in the area before and up to their last appearance datums of 2.55 and 2.78 Ma, respectively. Similarly, at Deep Sea Drilling Project (DSDP) Site 155 in the Panama Basin, Bukry (1973a) was unable to find either *D. surculus* or *D. tamalis*. He did, however, resolve the time interval represented by the *D. tamalis* subzone (CN12a) utilizing the occurrence of *Thoracosphaera saxeae* and the absence of *Reticulofenestra pseudoumbilica*.

140–422 mbsf (Lithologic Units U3 and U4)

Calcareous nannofossil diversity and abundance increase markedly and preservation quality improves from 140 mbsf to the base of the hole at 422 mbsf (Table T1). This corresponds to the nannofossil ooze interval discussed previously in this section. Thirteen datums are observed in this interval (Table T1). All thirteen datums are considered very reliable. They all occur in well-preserved, abundant intervals with high species diversity. Each index fossil is abundant when it is encountered, and each follows the other in a very predictable sequence.

Five expected datums were not observed between 140 and 422 mbsf; thus, the zones that are defined by these datums cannot be delineated. The bottom and top of *Amaurolithus primus*, corresponding to 7.2 and 4.8 Ma, respectively, were not observed. *Amaurolithus primus* was observed in one sample only at ~1 specimen per 100 fields of view (rare). *Amaurolithus amplificus* (LOD = 5.9 Ma) was observed in only one sample, and its abundance is recorded as rare. Likewise, the zones defined by these datums have been combined (Table T1) because the individual zones in this interval (NN16, NN15, NN14, and NN13) cannot be resolved. At DSDP Site 155, Bukry (1973a) also faced similar problems in resolving these zones because of the absence or scarcity of the marker species.

Catinaster calyculus and *Catinaster coalitus*, with corresponding FODs of 10.7 and 11.3 Ma, respectively, were not observed at Site 1039 or at any other Leg 170 site (the FOD of *C. coalitus* defines the base of CN6 or NN8; thus, Zones NN7 and NN8 could not be differentiated). Another species, *Calcidiscus macintyreai*, with an LOD of 1.59 Ma and an FOD of 15.6 Ma was also not observed. For this study, one of the characteristics adopted for calcidiscids is from E. DeKaenel (pers. comm., 1998), who has shown that there is a bimodal distribution of the *Calcidiscus* species and that to be considered *C. macintyreai* the specimen must be at least 11 µm in diameter. Only a few *Calcidiscus* species in the Leg 170 cores had a greater diameter; none was a top or bottom that represented a first or last occurrence.

The base of the cored sequence at Site 1039 consists of gabbro intruded into a calcareous diatomaceous ooze and breccia. Gabbro is present with the ooze in the basal core of Hole 1039B and in Cores 170–1039C-2R through 7R (Fig. F7). Reliable age-diagnostic calcareous nannofossils (*Sphenolithus heteromorphus* and *Helicosphaera ampliaperta*) are present in all samples taken from those cores (Table T1). They are reliable because they occur in a thick interval of consistently very abundant nannofossils (offering high stratigraphic resolution and no barren intervals) that exhibit good preservation. If the gabbro is indeed basement rock, then the age must be between 15.6 and 18.2 Ma. Hey (1977) and Lonsdale and Klitgord (1978) have suggested that the age of the

Cocos plate entering the subduction zone is between 25 and 27 Ma. However, Wilson (1996) has implied a younger age for the subducting lithosphere (Kimura, Silver, Blum, et al., 1997). Sediments examined during Leg 138, ~400 miles west of Site 1039, suggested ages of 15–17 Ma for the basement at Site 844. If that is the case, then at average East Pacific Rise spreading rates, the age of basement at Site 1039 could be between 21 and 25 Ma.

Site 1040

Site 1040 is located along seismic line CR-20 on the landward side of the Middle America Trench on the Caribbean plate at a water depth of ~4178 m, which is about 3.13 km from Site 1039 and ~1.6 m upgradient from the toe of the slope (Figs. F1, F2, F4). Three holes were cored through a deformed hemipelagic sedimentary wedge and the décollement and into the same three hemipelagic and pelagic sediment units and one oceanic basement unit cored at reference Site 1039 (Fig. F7) on the Cocos plate that has underthrust the Caribbean plate at Site 1040. A total composite penetration of 665 mbsf was achieved.

A composite diagram of total core recovery, lithology, depth cored, and age is illustrated in Figure F7. Hole 1040A penetrated 9.5 m of sediment recovered in one core. Hole 1040B penetrated to 190.2 mbsf, recovering 22 cores at a recovery rate of 67.3%. Hole 1040C was drilled to 159.3 mbsf before coring began. Fifty-three cores were taken from Hole 1040C, penetrating 505.7 m below 159.3 mbsf. Total core recovery at Hole 1040C was 74.6%.

Four sedimentary units and one igneous lithologic unit were recovered at Site 1040 (Fig. F7). Those units that make up the sedimentary wedge extend from 0 to 371 mbsf and are designated with a "P" for prism. From 371 to 653 mbsf, the same lithologic units cored at Site 1039 are present and are designated "U" for underthrust.

Lithologic Unit P1 extends from the seafloor to a depth of 371 mbsf. This unit comprises all of the prism section overlying the underthrust sections. Carbonate sediments and nannofossils are rare in Unit P1, as are diatoms, foraminifers, and radiolarians. Unit P1 consists primarily of massive silty clay to claystones interbedded with a few thin sandy layers. Slump features and breccia within the upper part of Unit P1 are suggestive of mass downslope transport processes. The lack of clear grading or bedding, the presence of slump folds, and the few bedded sands (turbidites) in the prism sediments indicate that most, if not all, of the prism has been mixed and reworked. This, of course, increases the difficulty in dating the prism sediments with fossils. The décollement is recognized at Site 1040 as a shear zone between Cores 170–1040C-19R through 23R. The bottom of the décollement is sharply defined at a depth of 371 mbsf. The top of the décollement is uncertain due to poor core recovery.

Beneath the décollement, lithology changes sharply from the massive silty clays and claystones characteristic of the prism to the clayey diatomite of lithologic Unit U1 first delineated at Site 1039. Figure F7 compares the underthrust units at Site 1039 (before subduction) to the same units at Site 1040 (after subduction). The lithology of the underthrust lithologic units are discussed in detail in "Site 1039," p. 5, and will not be repeated here. One of the few features found in the Site 1040 underthrust section not seen in the Site 1039 cores is the presence of small-scale faults and intervals of significant dip, indicating small-scale folding. The major difference in the lithologic sequence between the

two sites is in the thickness of the corresponding lithologic units. Lithologic Units U1 and U2 at Site 1040 are ~67% of the thickness of the corresponding units at Site 1039. Unit U3 at Site 1040 is ~80% of the thickness of corresponding Unit U3 at Site 1039.

Interestingly, the base of the sedimentary section U3C, located just above the gabbro intrusion, exhibits an increase in deformation. Shipboard structural geologists believe that this deformation is caused by near-ridge tectonics “very early in the sediment history” (Kimura, Silver, Blum, et al., 1997).

Nannofossil Distribution, Abundance, Preservation, and Chronology from Site 1040 Composite Section

The distribution, abundance, and preservation of calcareous nannofossils recovered from Holes 1040B and 1040C correlated to the nannofossil zonation scheme of Martini (1971) are presented in Tables **T2** and **T3**. An age-depth diagram plotting the age of all observed nannofossil datums at Site 1040 against the depth of observation is presented in Figure **F9**.

0–371 mbsf (Lithologic Unit P1)

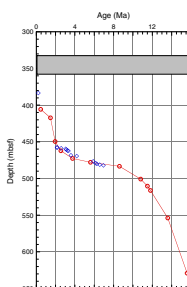
Relatively thin intervals of mixed Pleistocene, Pliocene, and middle and late Miocene calcareous nannofossil assemblages are characteristic of the 371-m-thick silty clay wedge section at Site 1040. Approximately 72% of the intervals analyzed in the upper 303 m of Unit P1 are barren. The longest nannofossil-barren interval, from 180.7 to 215.14 mbsf, coincides remarkably well with a zone of low chloride content in the pore waters. This zone, centered at 200 mbsf, contains pore waters that are up to 29% more diluted (chloride = 400 mM) than normal seawater (Kimura, Silver, Blum, et al., 1997), indicating that a conduit of low-chloride fluid advected from deeper in the wedge. It is likely that this low-chloride pore-water conduit has contributed to the absence of nannofossils and the paucity of diatoms characteristic of this horizon. In fact, comparison of the Holes 1040B and 1040C nannofossil distributions (Tables **T2**, **T3**) with the concentration of chloride with depth profiles in figure 24 (pg. 131) of Kimura, Silver, Blum, et al. (1997) indicates that most, if not all, of the nannofossil-barren zones at this site are associated with low-chloride concentration pore waters.

Within the nannofossil-bearing intervals, Pliocene through middle Miocene nannofossil reworking is ubiquitous (Table **T2**). Because index nannofossils observed from the wedge are rare or absent and because of the intense degree of reworking, all wedge age assignments must be considered conditional.

Careful study of the relatively few nannofossil-bearing intervals in Unit P1 indicates that from 0 to 14.25 mbsf (Section 170-1040B-3X-CC), the sediments are late Pleistocene in age based on a nannofossil assemblage characteristic of calcareous nannofossil Zone NN21 (Table **T2**). Zone NN21 is defined as extending from the FOD of *E. huxleyi* (260 ka to present). Thus, between 0 and 14.25 mbsf, the sediments are tentatively considered to be younger than 260 ka. From 14.25 to 303.91 mbsf (Section 170-1040C-15R-CC), the nannofossil assemblages cannot be zoned, although the assemblages are also characteristic of Pleistocene assemblages (Zones NN20 or NN19).

D. brouweri is first seen at 305.68 mbsf in Sample 170-1040C-16R-2, 48–50 cm, working downsection (Table **T3**). The LOD of *D. brouweri* defines the top of nannofossil Zone NN18 and also the top of the

F9. Age-depth relationship of calcareous nannofossil datums from the underthrust lithology of composite Holes 1040B and 1040C, p. 32.



Pliocene. Although its abundance is rare in this sample and to a depth of 317.58 mbsf, this interval is tentatively assigned to late Pliocene nannofossil Zone NN18. Within the deformed sedimentary wedge (0–330 mbsf), numerous normal and reversed polarity intervals have been determined. Lack of good biostratigraphic control and the high probability of thrust faults within the deformed sedimentary wedge have so far prevented a unique assignment of the reversal stratigraphy to any specific portion of the section.

The décollement at Site 1040 lies between Samples 170-1040C-19R-2, 37–39 cm, (334 mbsf) and 22R-CC (371 mbsf) (Table T3). Within this 37-m interval, only 23% of the total range contains nannofossils. The nannofossil assemblages in the décollement are very poorly preserved and rare to very few in number. Based solely on the nannofossil assemblage, this interval cannot be dated.

371–483 mbsf (Lithologic Unit U1)

Directly underlying the décollement at Site 1040 is the underthrust extension of lithologic Unit U1 first described from the Site 1039 reference section (Table T1). Thus, as expected, the nannofossil assemblages described from Site 1040 Unit U1 are nearly identical to those described for Site 1039 Unit U1.

From 371 to 404.81 mbsf, it is impossible to distinguish between latest Pleistocene to Holocene Zone NN21 from Zone NN20 because of the scarcity of all nannofossil species. Those species that are present are typically Pleistocene and extant, with no reworking present.

The top of *P. lacunosa* is observed at 405.74 mbsf and represents the top of early middle Pleistocene Zone NN19. The interval from 405.74 to 446.73 mbsf is assigned to Zone NN19. Nannofossils continue to be very scarce and poorly preserved in this interval. No reworking is apparent (Table T3).

D. brouweri is first observed at a depth of 449.8 mbsf. The LOD of *D. brouweri* defines the top of Zone NN18. Sediments from this level down to a depth of 459.4 mbsf are assigned to Zone NN18 (Table T3). Nannofossils in this interval are common to abundant. This indicates a change in lithology from the clayey diatomite of Unit U1, characteristic of the sediments between 371 and 422 mbsf, to the carbonate-bearing claystone of Unit U2 (Fig. F7).

Pliocene Zone NN17 is recognized in only one sample, at a depth of 462.4 mbsf, with the occurrence of the top of *D. pentaradiatus* (Table T3). Below this depth is a 10-m barren interval, which can only be assigned to the combined Pliocene Zones NN17–NN16. NN16 is defined by the LOD of *Discoaster surculus* to the LOD of *D. pentaradiatus*. Pliocene Zone NN15 is defined by the LOD of *R. pseudoumbilica* and/or the LOD of *Sphenolithus*. The tops of *R. pseudoumbilica* and *Sphenolithus* are observed at 472.75 mbsf, immediately below the 10-m barren interval. Although the LOD of *D. surculus* is not observed in the Site 1040 cores, if present, it should be observed in the 10-m barren interval.

The interval from 472.75 to 477.99 mbsf can only be assigned to undifferentiated Pliocene Zones NN15–NN12 because of the absence of several key FODs and LODs. *Amaurolithus tricorniculatus*, *Discoaster asymmetricus*, *A. primus*, *Ceratolithus rugosus*, *Ceratolithus acutus*, and *Triquetrorhabdus rugosus*, all key markers in defining the tops and/or bottoms of Pliocene Zones NN15, NN14, NN13, and NN12, are not observed in the Site 1040 cores (Table T3). Otherwise, nannofossils tend to be common to abundant in this interval. In the corresponding Site 1039 interval, Zones NN15–NN13 could not be differentiated because

of the sporadic occurrence of the index species within that particular interval. At Site 1039, all of the marker species are scarce (Table T1).

The top of *Discoaster berggrenii* is observed at 477.99 mbsf and marks the top of Zone NN11, the top of the late Miocene, and at this site, the top of lithologic Unit U3. Lithologic Unit U3 extends to 653.53 mbsf and consists primarily of siliceous nannofossil chalk (Fig. F7). Nannofossils are generally abundant to highly abundant in this entire interval and are moderately to well preserved. Late Miocene Zone NN11 extends to 491.39 mbsf (Table T3).

The interval from 491.39 to 498 mbsf is assigned to late Miocene Zones NN10 through the top of NN9. The top of *Coccolithus miopelagicus*, present at 498 mbsf, corresponds to an LOD of 10.8 Ma, lying just above the base of Zone NN8. The top and bottom of *Discoaster kugleri* are located at 510 and 536.51 mbsf, respectively. The range between the FOD (11.8 Ma) and LOD (11.5 Ma) of *D. kugleri* may be used to approximate Zone NN7 in the absence of other markers. Thus, the interval between the top of *D. kugleri* and the top of *C. miopelagicus* (501–507 mbsf) can be assigned to either Zone NN8 or NN7. The interval from 510 to 536 mbsf is assigned to Zone NN7 (Table T3).

The difficulty in delineating Zones NN10–NN7 in these cores is due to the absence of *Discoaster hamatus*, *D. surculus*, *Discoaster neorectus*, and *C. coalitus*, which are all species used to define the tops or bottoms of these zones. In the corresponding Site 1039 lithologic interval, these species, while present, are very scarce with the exception of *C. coalitus*, which is not seen at Site 1039 either (Table T1).

The LOD of *S. heteromorphus* (13.6 Ma) defines the base of Zone NN6 and the top of Zone NN5. The top of *S. heteromorphus* is observed at 553.94 mbsf. This places Zone NN6 from 536.51 to 553.94 mbsf. Zone NN5 extends from 553.94 to 629.2 mbsf, the top of *H. ampliaperta*. The bottom of Zone NN5 is defined by the LOD of *H. ampliaperta* (15.6 Ma) (Table T3).

Zone NN4 is a gap zone defined by the LOD of *Sphenolithus belemnos* (18.2 Ma) to the LOD of *H. ampliaperta*. *S. belemnos* was not observed at Site 1040, nor was the FOD of *H. ampliaperta* or the FOD of *S. heteromorphus*. Thus, Zone NN4 extends from 629.2 mbsf to the bottom of the cored sedimentary sequence (653.52 mbsf) (Table T3).

Sediments in the bottom 9 m of Unit U3C of Hole 1040C are poorly preserved and not as diverse or abundant as seen upsection in lithologic Units U2B and U3, where assemblages are relatively well preserved, and very abundant to highly abundant. The bottom of Hole 1040C consists of 7.4 m of gabbro (Fig. F7).

The base of the sedimentary section just above the gabbro intrusion exhibits increased deformation, which shipboard structural geologists believe occurred shortly after sedimentation. If this is the case, then the gabbro cored here may represent basement that is between 15.6 and 18.2 Ma.

Site 1041

Site 1041 is located on the landward side of the Middle America Trench on the Caribbean plate at a water depth of ~3306 m, ~12 km landward (midslope) from the toe of the wedge and 10.8 km landward from Site 1040 (Figs. F1, F3, F4). A 500- to 600-m-thick sedimentary apron overlies the prism section at this location (Figs. F3, F7). Three holes were cored into the sedimentary apron, but the target depth of

550 m into the prism was not met. However, a total composite penetration of 423.8 mbsf was achieved.

A composite diagram of total core recovery, lithology, depth cored, and age of the three Site 1041 holes is illustrated in Figure F7. Hole 1041A penetrated 155.1 mbsf of apron sediments and recovered 18 cores. Total core recovery from Hole 1041A was 74.4%. Hole 1041B penetrated 395.6 mbsf and recovered 25 cores at a recovery rate of 55.4%. Hole 1041C was drilled to 395 mbsf before coring began. Three cores were taken from Hole 1041C, penetrating another 28.8 m beyond 395 mbsf. Total core recovery at Hole 1041C was 23.8%.

Shipboard sedimentologists have characterized the entire cored sequence below Core 170-1041A-2H as poor quality because of extensive drilling disturbance and large sections of rubble that strongly suggested considerable upper hole cavings (Kimura, Silver, Blum, et al., 1997). This, of course, has severe implications for all age dating attempts and is taken into account in the determination of the nannofossil biostratigraphy presented later in this study. Also in many sections, particularly from Cores 170-1041A-15X through 170-1041B-20R (350 mbsf), gas hydrate dissociation has obliterated sedimentary structures (Kimura, Silver, Blum, et al., 1997).

Only one lithologic unit comprises the entire interval drilled and cored at Site 1041 (Fig. F7). This unit is designated apron Unit A1. Unit A1 is divided into two smaller units: Subunit A1A is mostly clays and silts and Subunit A1B is coarser, made up mostly of silts and sands. Carbonate preservation is spotty in both units. Calcareous nannofossils are sufficiently abundant, however, to record a fairly good biostratigraphic record from the Site 1041 cores, despite widespread reworking of the sediments. Micritic calcite and dolomite rhombs are present in almost every observed sample from ~15 mbsf to the base of Unit A1, increasing in abundance downhole.

Nannofossil Distribution, Abundance, Preservation, and Chronology from Site 1041 Composite Section

The distribution, abundance, and preservation of calcareous nannofossils recovered from Holes 1041A, 1041B, and 1041C correlated to the nannofossil zonation scheme of Martini (1971) are presented in Table T4. An age-depth plot is not possible because of the many limitations discussed below. However, a table of the range of ages with depth has been constructed from the nannofossil distribution data (Table T9).

0–273.83 mbsf (Lithologic Subunit A1A)

There is little doubt that reworking of species occurs everywhere in the Site 1041 cores. An attempt has been made on the range-distribution chart to separate the reworked species from those deemed to be in situ to arrive at a meaningful biostratigraphy for Site 1041. Table T4 summarizes this attempt; however, it is cautioned that all zones and all nannofossil datums observed are only *relatively* reliable. Conditions within this interval that contribute to the degree of reliability of the datums and zones are extensive reworking of older species, downhole contamination caused by cavings, and long intervals within the entire sequence that are barren of nannofossils, which severely limits the placement of observed tops and bottoms.

Nevertheless, taking into account all of the composite section's limitations to exacting an accurate determination of tops/bottoms, ages, and zonations at Site 1041, five ranges of nannofossil zones—or five di-

T9. Nannofossil zone assigned to depth observed in apron sediments from Site 1041, p. 62.

visions of time—are recognized. Referring to the Site 1041 nannofossil range chart in Table T4 and the nannofossil zone definitions outlined in Table T8 will aid in understanding how each assigned range of nannofossil zones in this unit have been determined.

The interval from the top of the composite hole to a depth of 2 mbsf is assigned to combined nannofossil Zones NN21–NN19. This implies that the sediments may be <260 ka or as old as 1.95 Ma.

A relatively long interval, extending from 5 to 14.03 mbsf, is essentially barren of nannofossils but may be assigned to combined Zones NN21–NN17. The assignment restricts the age of this interval from <260 ka to as old as 2.55 Ma.

The interval from 14.03 to 134.25 mbsf is characteristic of nannofossil Zones NN18–NN16 relative to what is recognized both upsection and downsection. This interval may not be younger than 1.95 Ma or older than 3.75 Ma.

Samples in the interval from 137.17 to 275.21 mbsf may be assigned to combined nannofossil Zones NN16–NN11. This zonation represents a relatively longer length of time than the overlying intervals and indicates that this interval may be no younger than 3.75 Ma and no older than 8.6 Ma.

The interval from 280.7 to 415.54 mbsf can only be determined to be older than Zone NN11, or 8.6 Ma, which is the FOD of *D. berggrenii*.

Site 1042

Site 1042 is located at a water depth between 3593 and 3581 m on the Caribbean plate, landward of the Middle America Trench, ~7.5 km west of Site 1041 (Figs. F1, F4). Two holes were drilled and cored to a composite depth of 390.8 mbsf. Hole 1042A was spot cored; seven spot cores were taken over a depth of 240.1 mbsf (Fig. F7). Core recovery was 19.3%.

Hole 1042B was drilled to a depth of 316 mbsf and then cored to a depth of 390.8 mbsf. Eight cores were recovered from Hole 1042B with a recovery of 11.9%. Two lithologic units have been described from the composite section. Unit 1 consists of silty claystone to 163 mbsf and silty claystone and limestone from 201.7 to 240 mbsf and from 353.7 to 390.8 mbsf (Fig. F7). The intervals from 163 to 201.7 mbsf and from 240 to 316 mbsf were not cored.

Unit U2, from 316 to 342.9 mbsf, consists of a carbonate-cemented sandstone breccia above a multilithic breccia with a clayey-silt matrix present at 342.9–353.7 mbsf. From 353.7 mbsf to the base of the hole at 390.8 mbsf is a silty claystone that is interpreted as Unit I.

Nannofossil Distribution, Abundance, Preservation, and Chronology from Site 1042 Composite Section

Unfortunately, the top 250 mbsf at Site 1042 was spot cored every 50 m, so a complete biostratigraphy for that section is not obtainable. Seven rotary cores were recovered. Several wiper trips and hole sweeps were conducted while we attempted to recover Cores 170-1042A-6R and 7R, adding downhole contamination to an already overworked hole (Kimura, Silver, Blum, et al., 1997). Because of the considerable amount of reworking, downhole contamination, and poor core recovery, no age determination or reliable biostratigraphy is possible utilizing calcareous nannofossils. In fact, neither diatoms nor foraminifers are able to provide further information about the upper 250 mbsf.

A second hole (Hole 1040B) was rotary-drilled to ~313 mbsf and then cored to 383 mbsf (Fig. F7). Calcareous nannofossil age determinations for this interval can not be determined with any degree of confidence.

During shipboard analysis, there was a somewhat optimistic attempt to assign nannofossil zones to the Site 1042 sequence (see p. 202, table 6, in Kimura, Silver, Blum, et al. [1997]). Although several zones were tentatively recognized, they are far from conclusive and should not be considered accurate. That nannofossil distribution and abundance range chart (Table T5) is reproduced here without the zones assigned aboard ship. In spite of the minimal biostratigraphy accomplished, the nannofossil distribution does give some sense of superposition at Site 1042.

Site 1043

Site 1043 (water depth = 4321 m) is located 0.4 km northeast of the toe of the continental slope on the Caribbean plate and 2.06 km from Site 1039 on the Cocos plate across the Middle America Trench, along seismic line CR-20 (Figs. F1, F2, F4). Site 1043 was cored through the sedimentary accretionary wedge and the décollement and into the underthrust section initially described from the Site 1039 reference cores taken from the immediate seaward side of the trench on the Cocos plate. Only one hole was cored at Site 1043. Hole 1043A was continuously cored to a depth of 282.3 mbsf. Total core recovery was 79.6%.

Only one lithologic unit is defined from the wedge sediments from Hole 1043A (Fig. F7). Lithologic Unit T1 is composed of thick intervals of silty clay and clay extending from the seafloor to 150.7 mbsf. These sediments are very characteristic of poorly sorted submarine debris and finer-grained sediment flows. Scattered throughout the sediments are clasts of clay, nannofossil ooze, and siliceous clayey nannofossil ooze. Overall, nannofossil abundances range from few to abundant within this entire unit. The base of unit T1 is the décollement.

The décollement is defined in Hole 1043A as a zone of anastomosing, discontinuous polished fracture systems observed from Section 170-1043A-16X-2, 112 cm, to the bottom of 17X-2 (141.50–150.57 mbsf), although the base is not sharply defined (Kimura, Silver, Blum, et al., 1997) (Fig. F7). Diatom abundances increase from trace amounts within the décollement zone to common immediately below the base of the zone, between 149.36 and 157.55 mbsf (Kimura, Silver, Blum, et al., 1997).

Below the décollement in the underthrust sediments, three lithologic units are recognized (Fig. F7). Lithologic Unit U1 extends from 150.57 (a structurally placed base) to 193.95 mbsf. The 5.5-m-thick turbidite observed in Unit U1 at Site 1039 is not observed here. Here, Unit U1 is predominately a diatomaceous ooze with varying amounts of clay and carbonate (Kimura, Silver, Blum, et al., 1997). Nannofossils are common in this sequence.

Lithologic Unit U2, extending from 193.95 to 263.71 mbsf, is characterized by a marked decrease in biogenic sediments and an increase in clay-sized terrigenous sediments. The tops of Unit U2 at both Sites 1039 and 1043 exhibit the same changes in the biogenic and terrigenous components. Unit U2 was divided into Subunits U2A and U2B based on the presence of strata containing siliceous nannofossil ooze and calcareous clay, with nannofossils in the latter (Kimura, Silver, Blum, et al., 1997). Subunit U2B extends from 245.63 to 263.71 mbsf. In general,

there is an increase in nannofossil abundance from the top of Unit U2 to its base (Fig. F7).

Lithologic Unit U3 is composed of siliceous nannofossil ooze and extends from 263.71 to 282.3 mbsf. Unit U3 was subdivided at Site 1039 into Subunits U3A, U3B, and U3C based on variations in the biogenic component downcore. Because of the depth cored, only Subunit U3A is observed at Site 1043. The bottom of Subunit U3A was not reached at this site (Fig. F7). Nannofossils are very abundant with depth throughout most of this interval until 281.65 mbsf, where their abundance drops by approximately an order of magnitude.

Nannofossil Distribution, Abundance, Preservation, and Chronology from Site 1043

The distribution, abundance, and preservation of calcareous nannofossils recovered from Site 1043 correlated to the nannofossil zonation scheme of Martini (1971) is presented in Table T6. An age-depth diagram plotting the age of all observed nannofossil datums at Site 1043 with depth is shown in Figure F10.

0–150.57 mbsf (Lithologic Unit T1)

The entire Unit T1 is Pleistocene in age, based on the consistent observations of *Gephyrocapsa oceanica*, *Gephyrocapsa caribbeanica*, *H. sellii*, *P. lacunosa*, and *Helicosphaera neogranulata* in the cored sequence from the seafloor down to the base of the décollement at 150.57 mbsf. Nannofossil Zones NN21, NN20, and NN19 are recognized in Unit T1 (Table T6).

Nannofossil Zone NN21 extends from the seafloor to 7.99 mbsf, the observed top of *E. huxleyi* (FOD = 260 ka). Middle and late Pliocene reworked species are observed. Although less abundant, the number of reworked species seen in this interval equals the number of extant species observed.

From 7.99 to 28.2 mbsf, Zone NN20 is recognized by the absence of *E. huxleyi* and *P. lacunosa*. Preservation is very poor in this interval, and individual specimens are scarce. However, there appears to be enough of an assemblage to assign this interval a zone, despite moderate reworking of middle and late Miocene calcareous nannofossil species.

The top of *P. lacunosa* is observed at 29.76 mbsf. The LOD of *P. lacunosa* defines the base of Zone NN20 and the top of Zone NN19. Zone NN19 extends from 29.76 to 150.57 mbsf (base of décollement).

The base of Zone NN19 is defined by the LOD of *D. brouwerii*, which was not seen in Unit T1. Therefore, with reasonable certainty, Unit T1 appears to be entirely Pleistocene.

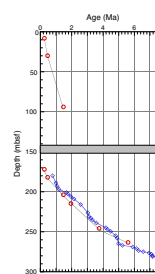
Carbonate clasts within Unit T1 were also analyzed for the presence of nannofossils. One clast at 92.05 mbsf contains a late Miocene Zone NN11 assemblage. Another clast, sampled at 129.66 mbsf, is typically early to middle Miocene Zone NN4. The nannofossil assemblage observed in this clast is identical to the assemblages observed in the oldest sediments cored at Sites 1039 and 1040 (Tables T1, T3).

The décollement extends from 140.5 to 150.57 mbsf. Nannofossils, although present and indicative of Zone NN4, are not common within the décollement zone.

150.57–263.71 mbsf (Lithologic Unit U2)

Five nannofossil zones are recognized in Subunit U2A, which extends from 150.57 to 245.63 mbsf. From 150.57 to 171.8 mbsf, late

F10. Age-depth relationship of calcareous nannofossil datums from Hole 1043A, p. 33.



Pleistocene–Holocene Zone NN21 is observed based on the occurrence of *E. huxleyi* at 171.8 mbsf. Two of the five samples taken at regular intervals in this zone are barren, and the preservation is generally poor to moderate (Table T6).

Nannofossil Zone NN20, established by the absence of both *E. huxleyi* and *P. lacunosa*, is assigned to the interval from 174.8 to 181.6 mbsf. Below this level, Zone NN19 is recognized by observing both the top of *P. lacunosa* at 181.89 mbsf and the top of *D. brouwerii* at 226.5 mbsf (Table T6).

Zone NN18, defined by the LOD of *D. pentaradiatus* to the LOD of *D. brouwerii*, cannot be delineated in the interval from 226.5 to 241.9 mbsf because the LOD of *D. pentaradiatus* is not observed at this site. The LOD of *D. surculus* is not observed either; this LOD defines the top of Zone NN16 and base of Zone NN17. *R. pseudoumbilica*, whose LOD defines the bottom of Zone NN16, is observed at 245.67 mbsf. Thus, the interval from 226.65 to 242.9 mbsf is assigned to undifferentiated Zones NN18–NN16. Nannofossils in this strata are typically few in number and poorly preserved. The base of Subunit U2A approximates the base of the strata assigned to Zone NN18–NN16 (Table T6).

At Sites 1039 and 1040, some difficulty exists in delineating Zones NN18–NN16 and NN15–NN12, a situation similar to that at Site 1043. The periods of time represented by these assemblages exhibit the lowest sedimentation rates (see Figs. F8, F9, F10).

Nannofossils in Subunit U2B are abundant and generally better preserved than those upsection in Subunit U2A and show identical assemblage characteristic trends observed in the Sites 1040 and 1039 underthrust sequences. Despite increased preservation and abundance, Zones NN15–NN12 cannot be resolved between 251.68 and 258.3 mbsf. Samples from that interval are assigned to undifferentiated Zones NN15–NN12. Recall that at Sites 1039 and 1040 in the underthrust sections the marker species in the Zones NN18–NN12 interval are scarce or not present. These include *A. tricorniculatus*, *A. primus*, *C. rugosus*, *D. asymmetricus*, and *T. rugosus* (Table T6).

Nannofossils in Unit U3 are very to highly abundant and diverse and generally exhibit good preservation (Unit U3 is a siliceous calcareous nannofossil ooze). At Site 1043, all of Unit U3 is placed in Zone NN11, which is defined as the FOD to LOD of *Discoaster quinqueramus*. Unlike the lithology cored at Sites 1039 and 1040, the base of Unit U3 was not reached at Site 1043.

SUMMARY

Three Pleistocene, five Pliocene, and thirteen late and middle Miocene calcareous nannofossil datums have been identified in the Leg 170 cored sequences. A summary table of these datums, their ages, and their locations in the Leg 170 cores is presented in Table T10. Whereas other datums were identified, the datums listed in this table are considered to be the most reliable.

What appears to be a complete—or nearly complete—late Pleistocene through early middle Miocene section (see below) is recognized in the calcareous nannofossil record. The oldest assemblages, observed at Sites 1039 and 1040, are latest early Miocene in age, nannofossil Zone NN4, with an absolute age assignment between 15.6 and 18.2 Ma. These assemblages are associated with gabbro intrusions into the basal sediments, indicating an age for the intrusion event between 15.6 and 18.2

T10. Composite summary of Pleistocene, Pliocene, and late and middle Miocene calcareous nannofossil datums, p. 63.

Ma at both Sites 1039 and 1040. One contact metamorphic hornfels sample contains relict nannofossils. Reference Site 1039, located on the Cocos plate, provides the best-preserved sequence of sediments from late Pleistocene to latest early Miocene in age. The sediments cored in the prism sections at Sites 1040, 1041, 1042, and 1043 all indicate that the age of nannofossil assemblages in the prism sediments, including the toe, wedge, and apron, are all of Pleistocene age with a considerable amount of upper Miocene reworking.

A period of low sediment accumulation rates is recorded for Pliocene sediments at Sites 1039, 1040, and 1043. Differentiating Pliocene Zones NN18–NN16 (equivalent to nannofossil Subzones CN12c, CN12b, and CN12a) could not be accomplished at any of these sites. Pliocene nannofossil Zones NN15, NN14, NN13, and NN12, which occur in the top of the early Pliocene and bottom of the late Pliocene, could not be resolved at any site either. In late Miocene sediments, nannofossil Zone NN11 was easily identified at all three sites; however, the four subzones within nannofossil Zone NN11 could not be resolved. Within the Miocene, nannofossil zones older than NN11 (equivalent to nannofossil Zones CN8–CN5b) were difficult to distinguish individually until Zone NN6 (equivalent to Subzone CN5a). These intervals, where the nannofossil zones were not resolved or were difficult to resolve, lie in an ~8.5 m.y.-long (2.5–11 Ma) low sediment accumulation rate time interval (Figs. F8, F9, F10). This interval has a sediment accumulation rate of ~5.3 m/m.y. Resolution of nannofossil, planktonic foraminifer, and diatom zones within this long section all suffer from the low sedimentation rates.

Interestingly, at DSDP Site 155 in the Panama Basin, Bukry (1973a) encountered many of the same difficulties encountered here in resolving the early Pliocene and late Miocene nannofossil Zones. Coccolith assemblages recovered from Site 155 also range in age from Pleistocene to late early Miocene. At DSDP Site 155, nannofossil Zones NN15–NN12 could not be resolved because of the absence of *Discoaster tamalis*, *D. surculus*, the amauroliths, *Ceratolithus amplificus*, *C. rugosus*, and *Triquetrorhadulus rugosus*.

Nannofossil Zones NN8 (equivalent to Zone CN 6) and NN7 (equivalent to Zone CN5b) are recognized at Site 155 in only 1 m of sediment. These zones were not resolved at any Leg 170 site because of the absence of *C. coalitus*. In fact, some of the zones inferred by Bukry (1973a) at Site 155 were determined with secondary markers.

It is noted that the closure of the Central American Isthmus (CAI) may have played a significant role in the plankton productivity of the overlying Leg 170 study area. The formation of the isthmus has been a complex process over the last 15 m.y. (Keigwin, 1982; Ruddiman and Raymo, 1988; Coates and Obando, 1996; Cronin and Dowsett, 1996), creating a total marine barrier by ~3.1–2.8 Ma. The closure of the isthmus has been tied to the initiation of Northern Hemisphere glaciation at 2.5 Ma and a revamping of both Atlantic and Pacific Ocean current flow regimes. The nannofossil data and conclusions drawn from this study will become the basis for a more comprehensive study into the effects of the formation of the CAI on Eastern Equatorial Pacific calcareous plankton.

ACKNOWLEDGMENTS

I would like to thank ODP for the opportunity to participate in Leg 170 as a paleontologist. I am grateful to Eli Silver and Gaku Kimura, the Leg 170 co-chiefs, for their leadership during Leg 170 and the rest of the scientific staff for the camaraderie and spirit in which they undertook this scientific endeavor. It was a pleasure to work with each of them. The same can be said about the technical staff and crew aboard the *JOIDES Resolution*. Thanks is also due to Marino Protti for organizing and leading a field trip to the ophiolite complex on the Nicoya Peninsula during our postcruise meeting. Woody Wise allowed full use of his laboratory for postcruise studies, and I thank him greatly for that. I would also like to thank Jason Chipp and Andy Feldman for slide preparation and Barbara Bruno for proofreading the galley proof. Last, but certainly not least, I am always appreciative of the ODP staff at College Station, Texas. This paper benefited from the reviews by Wuchang Wei, Diane Winter, and Woody Wise. This study was supported by a grant from USSAC.

REFERENCES

- Berggren, W.A., Hilgen, F.J., Langereis, C.G., Kent, D.V., Obradovich, J.D., Raffi, I., Raymo, M.E., and Shackleton, N.J., 1995a. Late Neogene chronology: new perspectives in high-resolution stratigraphy. *Geol. Soc. Am. Bull.*, 107:1272–1287.
- Berggren, W.A., Kent, D.V., Swisher, C.C., III, and Aubry, M.-P., 1995b. A revised Cenozoic geochronology and chronostratigraphy. In Berggren, W.A., Kent, D.V., Aubry, M.-P., and Hardenbol, J. (Eds.), *Geochronology, Time Scales and Global Stratigraphic Correlation*. Spec. Publ.—Soc. Econ. Paleontol. Mineral. (Soc. Sediment. Geol.), 54:129–212.
- Bukry, D., 1973a. Coccolith stratigraphy, eastern equatorial Pacific, Leg 16, Deep Sea Drilling Project. In van Andel, T.H., Heath, G.R., et al., *Init. Repts. DSDP*, 16: Washington (U.S. Govt. Printing Office), 653–711.
- _____, 1973b. Low-latitude coccolith biostratigraphic zonation. In Edgar, N.T., Saunders, J.B., et al., *Init. Repts. DSDP*, 15: Washington (U.S. Govt. Printing Office), 685–703.
- _____, 1975. Coccolith and silicoflagellate stratigraphy, northwestern Pacific Ocean, Deep Sea Drilling Project Leg 32. In Larson, R.L., Moberly, R., et al., *Init. Repts. DSDP*, 32: Washington (U.S. Govt. Printing Office), 677–701.
- Coates, A.G., and Obando, J.A., 1996. The geologic evolution of the Central American Isthmus. In Jackson, J.B.C., Budd, A.F., and Coates, A.G. (Eds.), *Evolution and Environment in Tropical America*: Chicago (Univ. of Chicago Press), 21–55.
- Cronin, T.M., and Dowsett, H.J., 1996. Biotic and oceanographic response to the Pliocene closing of the Central American isthmus. In Jackson, J.B.C., Budd, A.F., and Coates, A.G. (Eds.), *Evolution and Environment in Tropical America*: Chicago (Univ. of Chicago Press), 21–56.
- Hey, R., 1977. Tectonic evolution of the Cocos-Nazca spreading center. *Geol. Soc. Am. Bull.*, 88:1404–1420.
- Keigwin, L., 1982. Isotopic paleoceanography of the Caribbean and East Pacific: role of Panama Uplift in late Neogene time. *Science*, 217:350–353.
- Kimura, G., Silver, E., Blum, P., et al., 1997. *Proc. ODP, Init. Repts.*, 170: College Station, TX (Ocean Drilling Program).
- Lonsdale, P., and Klitgord, K.D., 1978. Structure and tectonic history of the eastern Panama Basin. *Geol. Soc. Am. Bull.*, 89:981–999.
- Martini, E., 1971. Standard Tertiary and Quaternary calcareous nannoplankton zonation. In Farinacci, A. (Ed.), *Proc. 2nd Int. Conf. Planktonic Microfossils Roma*: Rome (Ed. Tecnosci.), 2:739–785.
- Okada, H., and Bukry, D., 1980. Supplementary modification and introduction of code numbers to the low-latitude coccolith biostratigraphic zonation (Bukry, 1973; 1975). *Mar. Micropaleontol.*, 5:321–325.
- Perch-Nielsen, K., 1985. Cenozoic calcareous nannofossils. In Bolli, H.M., Saunders, J.B., and Perch-Nielsen, K. (Eds.), *Plankton Stratigraphy*: Cambridge (Cambridge Univ. Press), 427–554.
- Ruddiman, W.F., and Raymo, M.E., 1988. Northern hemisphere climatic regimes during the past 3 Ma: possible tectonic connections. *Philos. Trans. R. Soc. London B*, 318:411–430.
- Wilson, D.S., 1996. Fastest known spreading on the Miocene Cocos-pacific plate boundary. *Geophys. Res. Lett.*, 23:3003–3006.

TAXONOMIC APPENDIX

Species List in Alphabetical Order of Species Epithets

- Dictyococcites* Black (1967)
Helicosphaera Kamptner (1954) and *Helicopontosphaera*
Pontosphaera Lohmann, 1902
Reticulofenestra Hay, Mohler, and Wade (1969)
Sphenolithus abies Deflandre in Deflandre and Fert (1954)
Ceratolithus acutus Gartner and Bukry (1974)
Catinaster altus (Muller, 1974a) Perch-Nielsen (1984a)
Amaurolithus amplificus (Bukry and Percival, 1971) Gartner and Bukry (1975)
Helicosphaera ampliaperta Bramlette and Wilcoxon (1967)
Gephyrocapsa aperta Kamptner (1963)
Ceratolithus armatus Muller (1974a)
Discoaster asymmetricus Gartner (1969c)
Discoaster aulakos Gartner (1967)
Discoaster bellus Bukry and Percival (1971)
Discoaster berggrenii Bukry (1971a)
Discoaster bollii Martini and Bramlette (1963)
Discoaster brouweri Tan (1927) emend. Bramlette and Riedel (1954)
Helicosphaera burkei Black (1971a)
Discoaster calcaris Gartner (1967)
Gephyrocapsa caribbeanica Boudreaux and Hay (1969)
Helicosphaera carteri (Wallich, 1877) Kamptner (1954)
Discoaster challengerii Bramlette and Riedel (1954)
Rhabdosphaera clavigeri Murray and Blackman (1898)
Helicosphaera colombiana Gartner (1977b)
Ceratolithus cristatus Kamptner (1950)
Discoaster decorus (Bukry 1971b) Bukry (1973c)
Discoaster deflandrei Bramlette and Riedel (1954)
Pontosphaera discopora Schiller (1925)
Discoaster druggii Bramlette and Wilcoxon (1967)
Discoaster exilis Martini and Bramlette (1963)
Triquetrorhabdulus farnsworthii (Gartner, 1967) Perch-Nielsen (1984a)
Cyclicargolithus floridanus (Roth and Hay in Hay et al., 1967) Bukry (1971a)
Discoaster hamatus Martini and Bramlette (1963)
Sphenolithus heteromorphus Deflandre (1953)
Emiliania huxleyi (Lohmann, 1902) Hay and Mohler in Hay et al. (1967)
Helicosphaera hyalina Gaarder (1970)
Discoaster intercalaris Bukry (1971a)
Helicosphaera kampfneri Hay and Mohler in Hay et al. (1967)
Discoaster kugleri Martini and Bramlette (1963)
Pseudoemiliania lacunosa (Kamptner, 1963) Gartner (1969c)
Calcidiscus leptoporus (Murray and Blackman, 1898) Loeblich and Tappan (1978)
Discoaster loeblichii Bukry (1971a)
Calcidiscus macintyrei (Bukry and Bramlette, 1969b) Loeblich and Tappan (1978)
Catinaster mexicanus Bukry (1971b)
Reticulofenestra minuta Roth (1970)
Coccoolithus miopelagicus Bukry (1971a)
(Umbilicosphaera mirabilis Lohman, 1902) = *U. sibogae*
Discoaster moorei Bukry (1971b)
Sphenolithus moriformis (Bronnimann and Stradner, 1960) Bramlette and Wilcoxon (1967)
Pontosphaera multipora (Kamptner, 1948) Roth (1970)
Discoaster musicus Stradner (1959b)
Sphenolithus neoabies Bukry and Bramlette (1969a)
Helicosphaera neogranulata Gartner (1977b)
Discoaster neohamatus Bukry and Bramlette (1969b)
Discoaster neorectus Bukry (1971a)
Coronocyclus nitescens (Kamptner, 1963) Bramlette and Wilcoxon (1967)

- Gephyrocapsa oceanica* Kamptner (1943)
Coccolithus pelagicus (Wallich, 1877) Schiller (1930)
Discoaster pentaradiatus Tan (1927) emend. Bramlette and Riedel (1954)
Hayaster perplexus (Bramlette and Riedel, 1954) Bukry (1973d)
Discoaster prepentaradiatus Bukry and Percival (1971)
Amaurolithus primus (Bukry and Percival, 1971) Gartner and Bukry (1975)
Reticulofenestra pseudoumbilica (Gartner, 1967) Gartner (1969c)
Discoaster pseudovariabilis Martini and Worsley (1971)
Discoaster quinqueramus Gartner (1969c)
Helicosphaera rhomba Bukry (1971a)
Ceratolithus rugosus Bukry and Bramlette (1968)
Triquetrorhabdulus rugosus Bramlette and Wilcoxon (1967)
(*Discoaster sanmiguelensis* Bukry, 1981b)? = *D. musicus*
Helicosphaera scissura Miller (1981)
Helicosphaera sellii Bukry and Bramlette (1969b)
Umbilicosphaera sibogae (Weber-van Bosse, 1901) Gaarder (1970)
Discoaster signus Bukry (1971b)
Gephyrocapsa sinuosa Hay and Beaudry (1973)
Discoaster surculus Martini and Bramlette (1963)
Discoaster tamalis Kamptner (1967)
Ceratolithus telesmus Norris (1965)
Discoaster triradiatus Tan (1927)
Discoaster variabilis Martini and Bramlette (1963)
Sphenolithus verensis Blackman (1978)
Helicosphaera wallachii (Lohmann, 1902) Boudreux and Hay (1969)
Helicosphaera wilcoxonii Gartner (1971)
(Epithets from Perch-Nielson, 1985)

Figure F1. Location of Leg 170 Sites 1039, 1040, 1041, 1042, and 1043 along seismic reflection survey lines offshore from the Nicoya Peninsula. The location of the study area with reference to Central America and the eastern Pacific Ocean is shown in the inset (Kimura, Silver, Blum, et al., 1997).

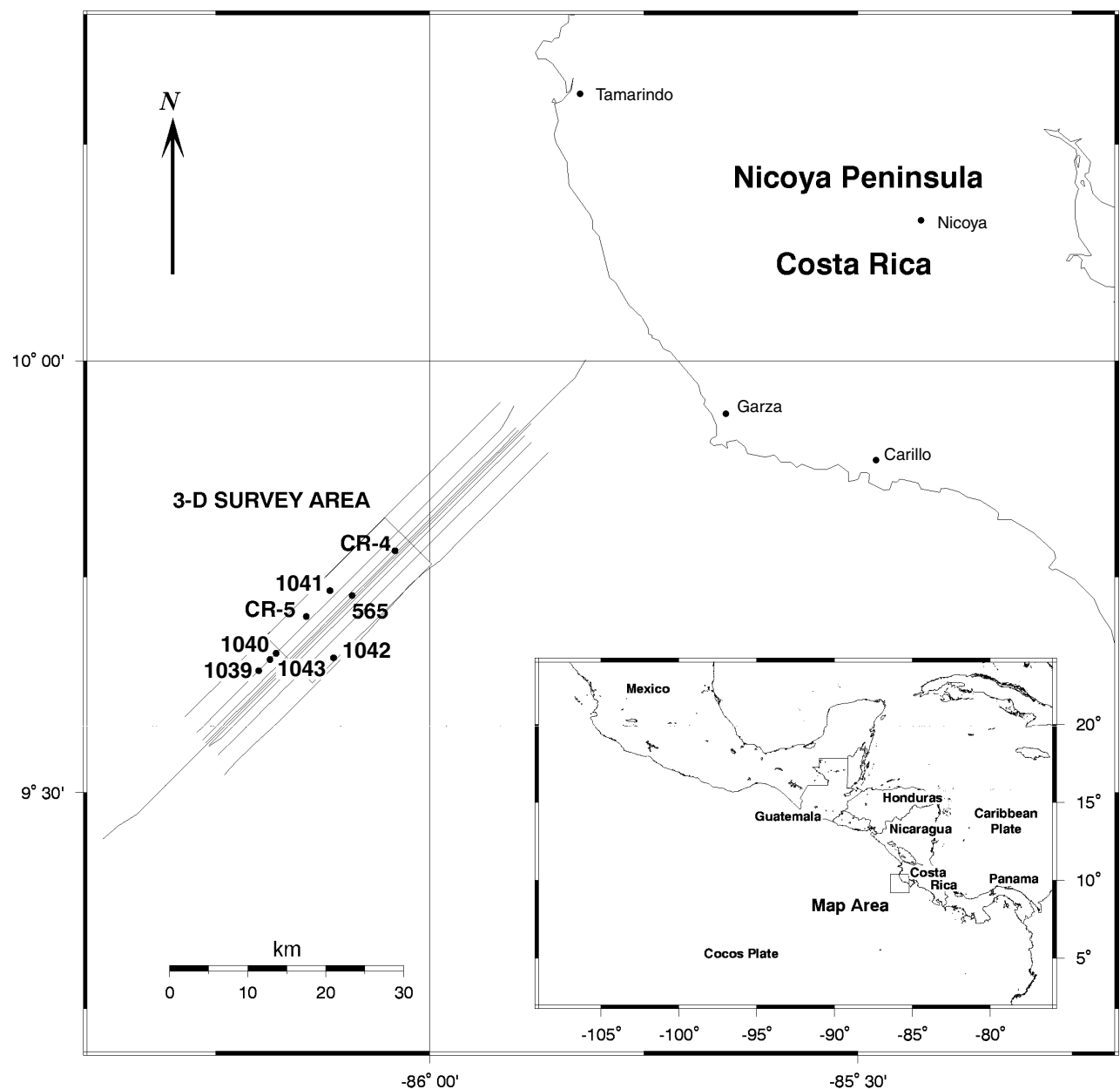


Figure F2. Two-dimensional seismic reflection profile CR-20 showing the locations of the Site 1039 reference section on the Cocos plate on the Middle America Trench floor and Sites 1040 and 1043 on the Caribbean plate. Particularly noticeable is the décollement surface, which lies between 4.35 and 4.55 km in this profile.

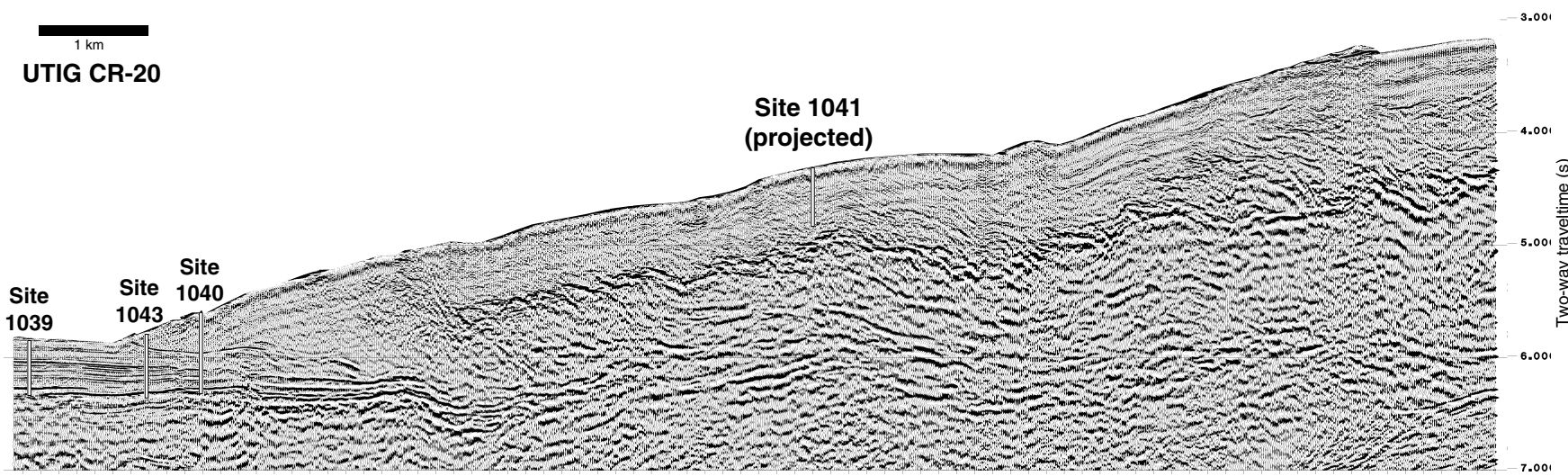


Figure F3. Two-dimensional seismic reflection profile CR-20 showing the projected location of Site 1041 relative to Sites 1039, 1040, and 1043.

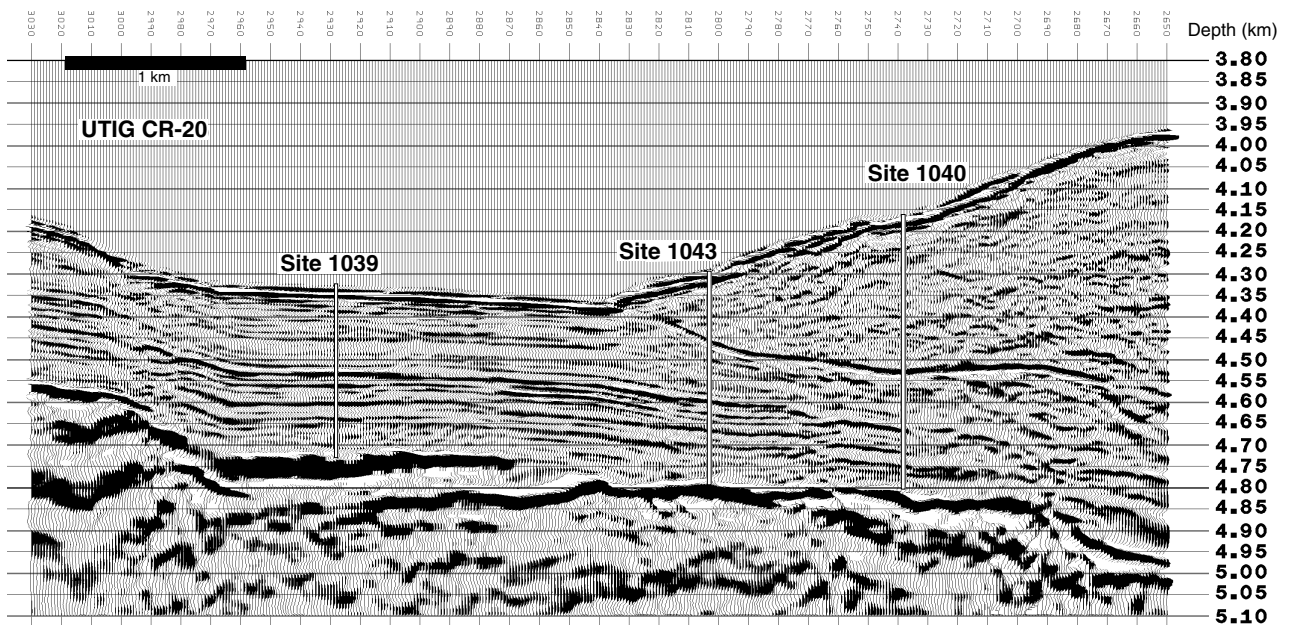


Figure F4. Bathymetric map of the Leg 170 study area showing the depths and locations of the five Leg 170 sites. Included are seismic reflection survey lines CR-20, on which Sites 1039, 1040, and 1043 are located, lines CR3D-48 and CR3D-450, on which Site 1042 is located, and lines CR3D-171 and CR3D-276, on which Site 1041 is located. The bathymetric contour interval is 20 m.

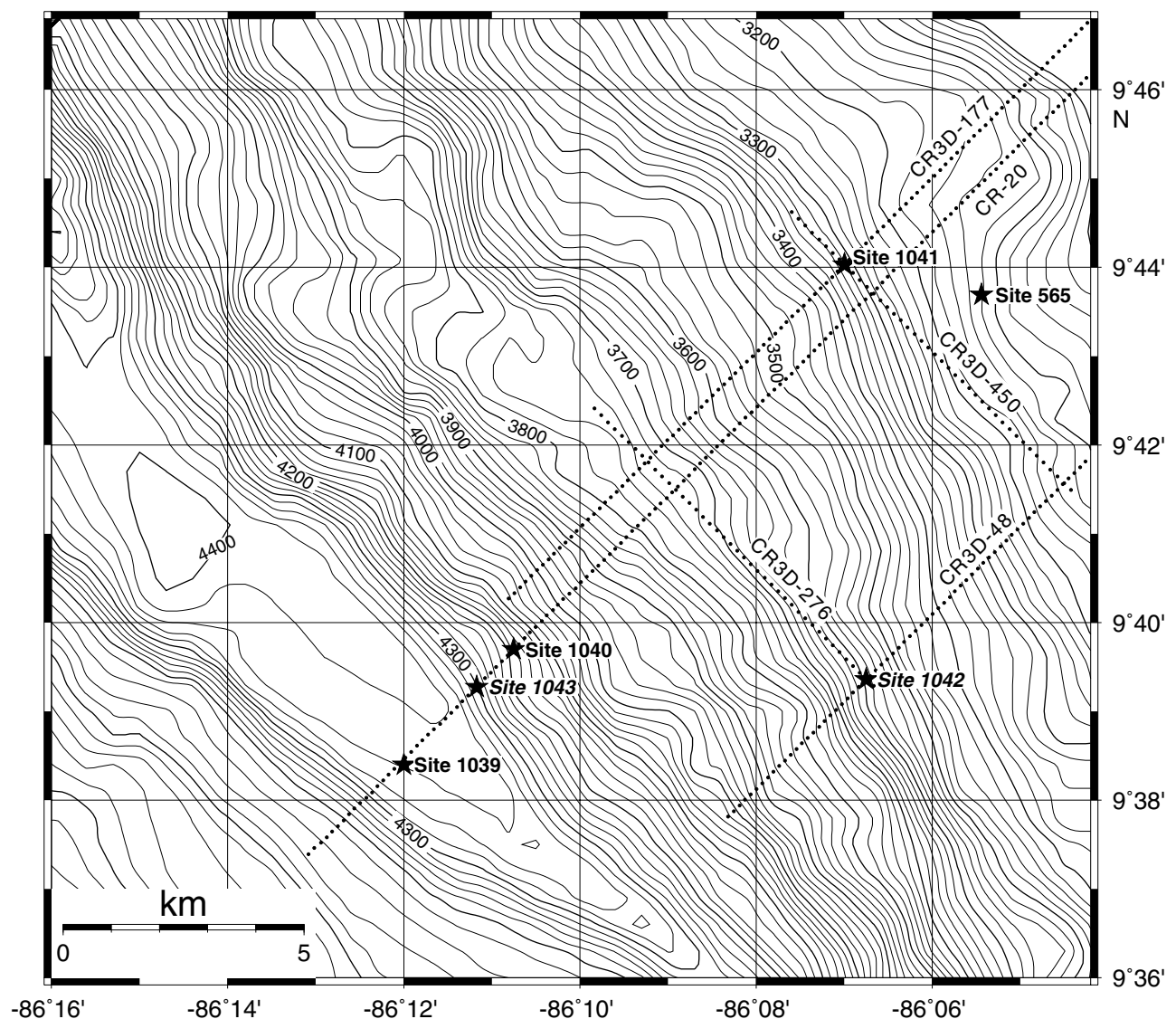


Figure F5. Geologic time scale illustrating the comprehensive correlation between the nannofossil zones of Martini (1971) and Bukry (1973a, 1975), used in this study, and the astronomical/geomagnetically derived chronologic scale of Berggren et al. (1995a, 1995b) for the Pleistocene and Pliocene.

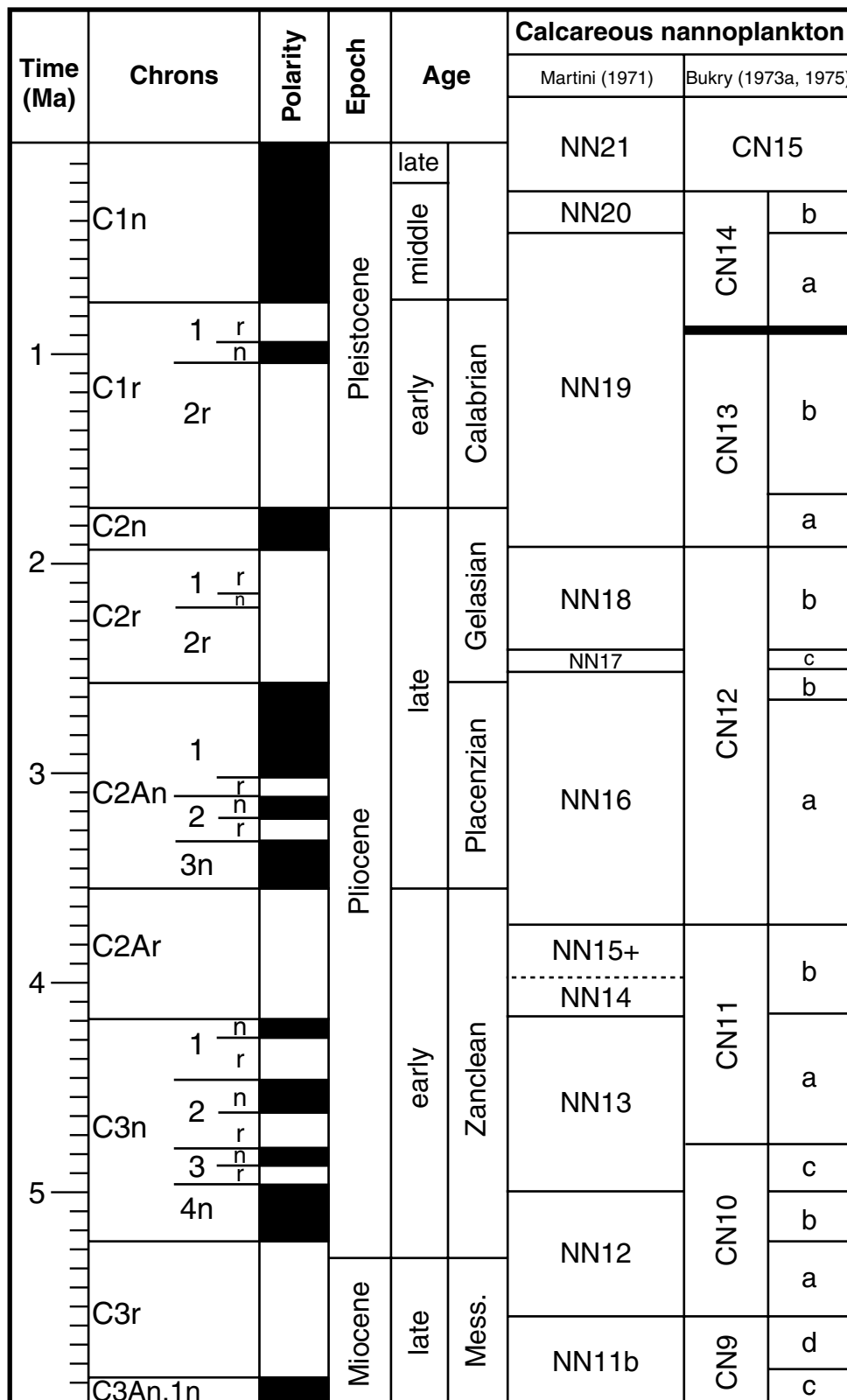


Figure F6. Geologic time scale illustrating the comprehensive correlation between the nannofossil zones of Martini (1971) and Bukry (1973a, 1975), used in this study, and the astronomical/geomagnetically derived chronologic scale of Berggren et al. (1995b) for the Miocene.

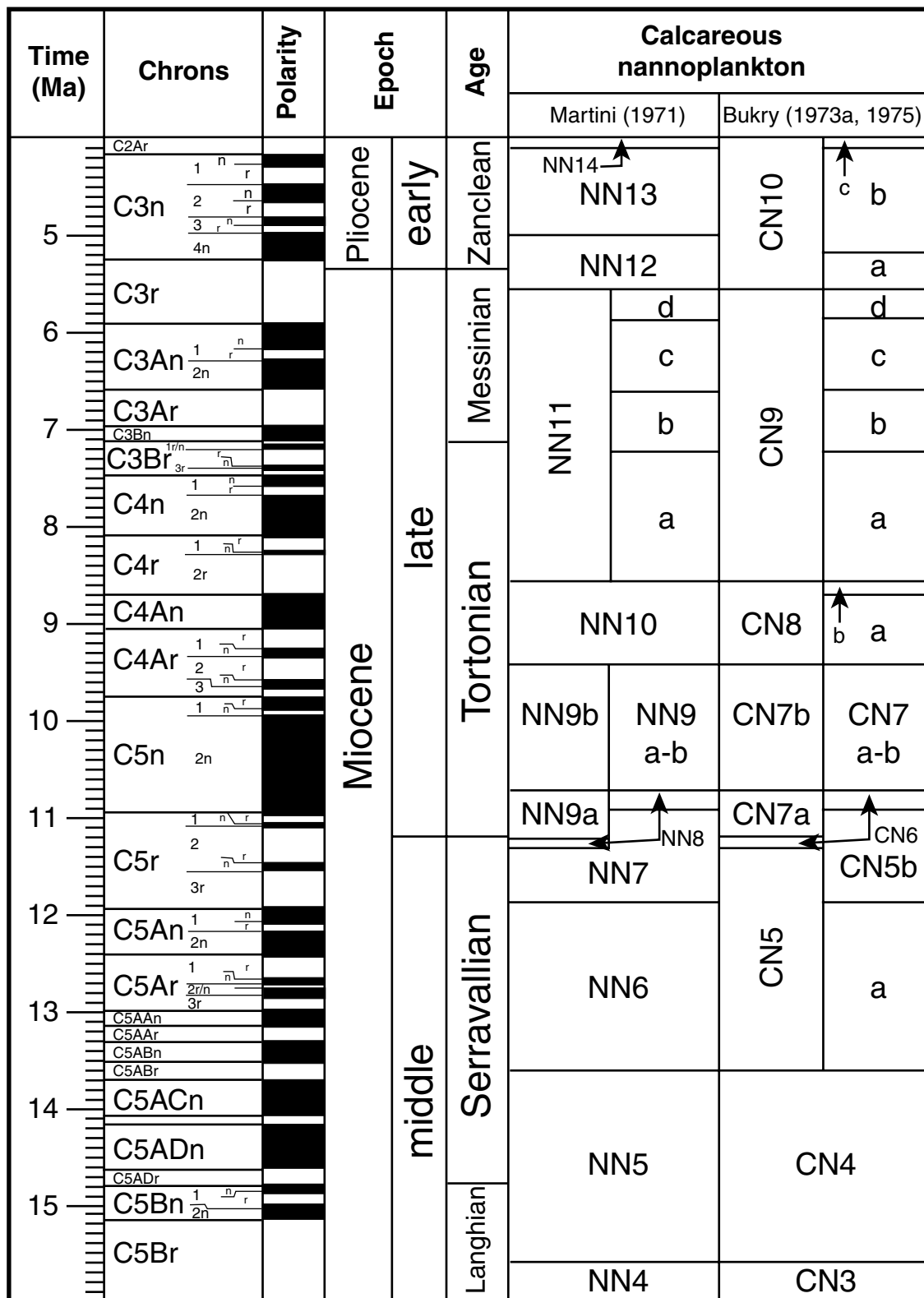


Figure F7. Stratigraphic profile of composite lithologic sections from Sites 1039, 1043, 1040, 1042, and 1041. The profile trends northeastward from Site 1039 to Site 1041. Site 1039 is immediately seaward of the Middle America Trench; Sites 1043, 1040, 1042, and 1041 trend northeastward, respectively, from the toe of the sedimentary wedge to the apron. Lithologic unit designations are as follows: U = underthrust units (or in the case of Site 1039, eventually will be an underthrust unit); T = toe sediments; P = prism sediments; and A = apron sediments. Sediment ages and core recovery are also shown. The age of the sediment from Site 1042 is highly suspect, resulting from a very optimistic shipboard analysis of seven spot cores (see “[Nannofossil Distribution, Abundance, Preservation, and Chronology from Site 1042 Composite Section](#),” p. 14, in “Leg 170 Calcareous Nannofossil Biostratigraphic Synthesis” for further discussion). ([Figure shown on next page.](#))

J.P. MUZA
CALCAREOUS NANNOFOSSIL BIOSTRATIGRAPHY

Figure F7 (continued).

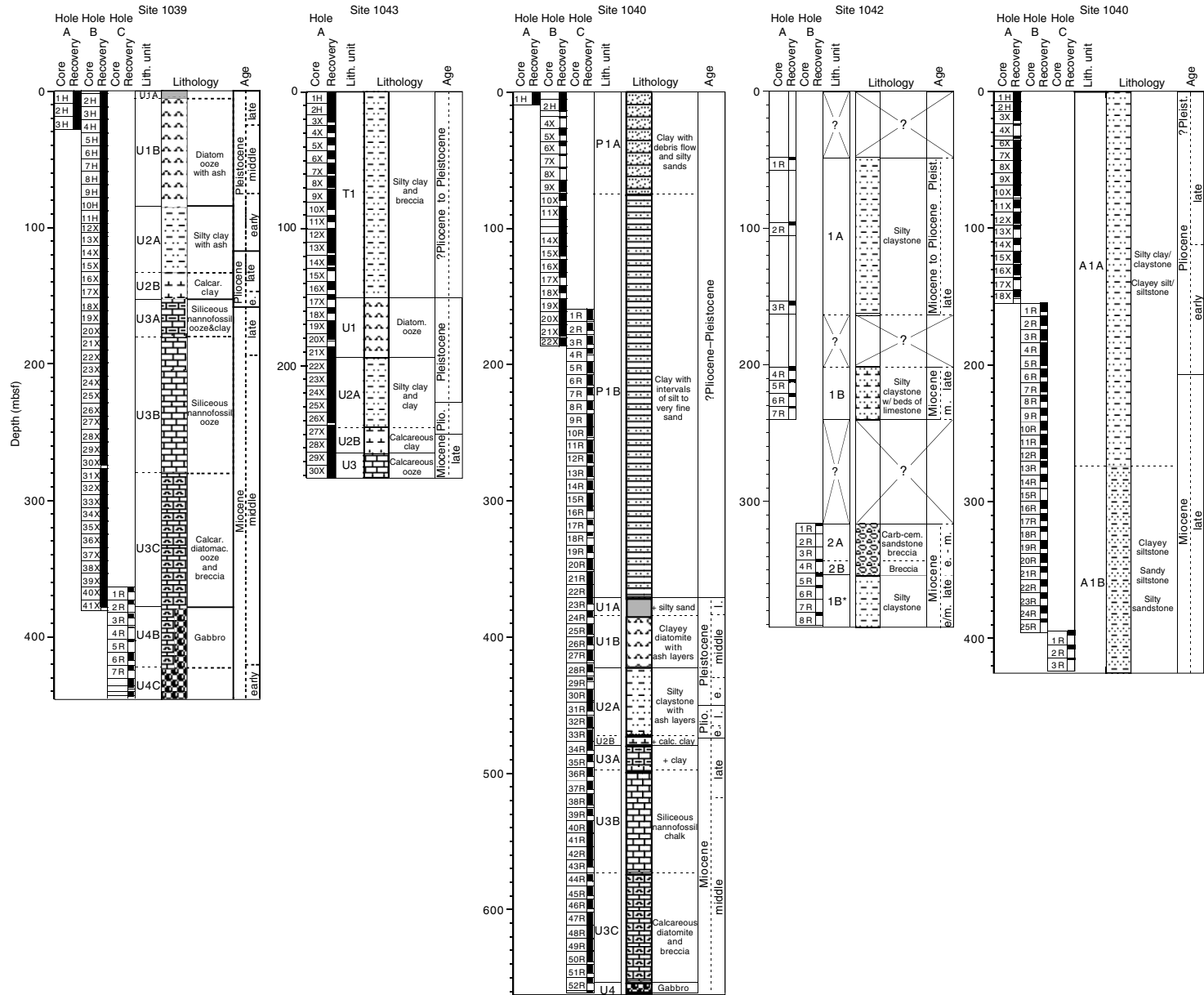


Figure F8. Age-depth relationship of calcareous nannofossil datums from the composite lithologic section of Holes 1039B and 1039C. Open circles = calcareous nannofossil datums; open diamonds = paleomagnetic data (Kimura, Silver, Blum, et al., 1997).

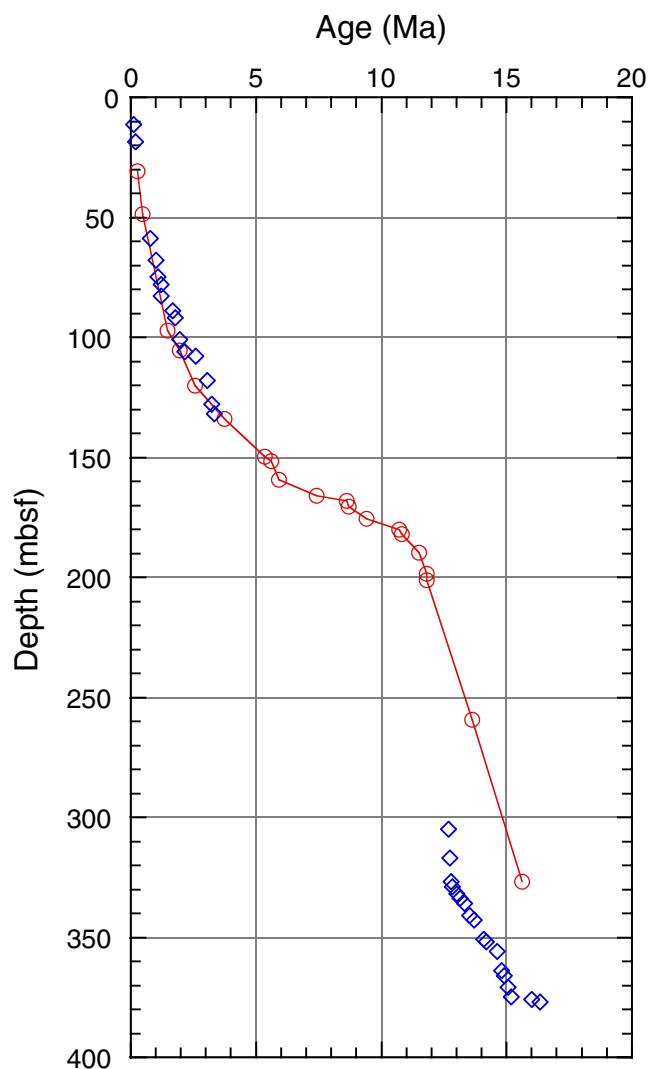


Figure F9. Age-depth relationship of calcareous nannofossil datums from the underthrust lithology of composite Holes 1040B and 1040C. Open circles = calcareous nannofossil datums; open diamonds = paleomagnetic data (Kimura, Silver, Blum, et al., 1997); and shaded area = décollement between 332 and 358 mbsf.

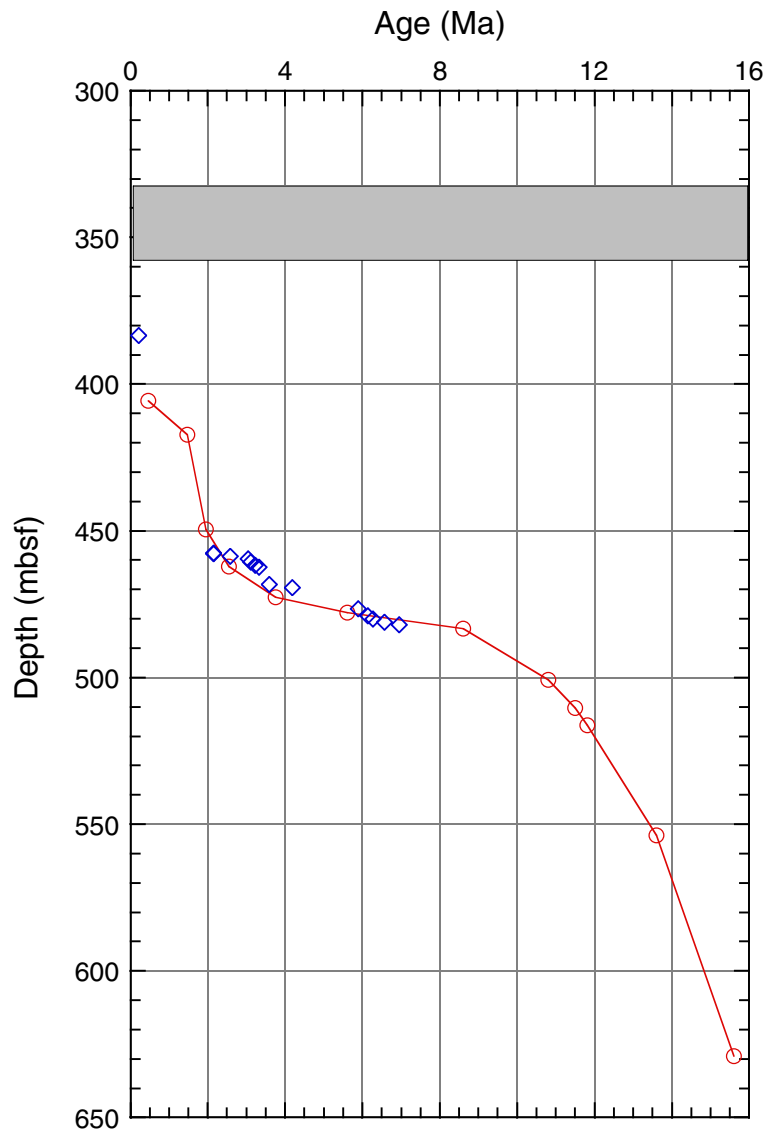


Figure F10. Age-depth relationship of calcareous nannofossil datums from Hole 1043A. Open circles = calcareous nannofossil datums; open diamonds = paleomagnetic data (Kimura, Silver, Blum, et al., 1997); and shaded area = décollement at ~150 mbsf.

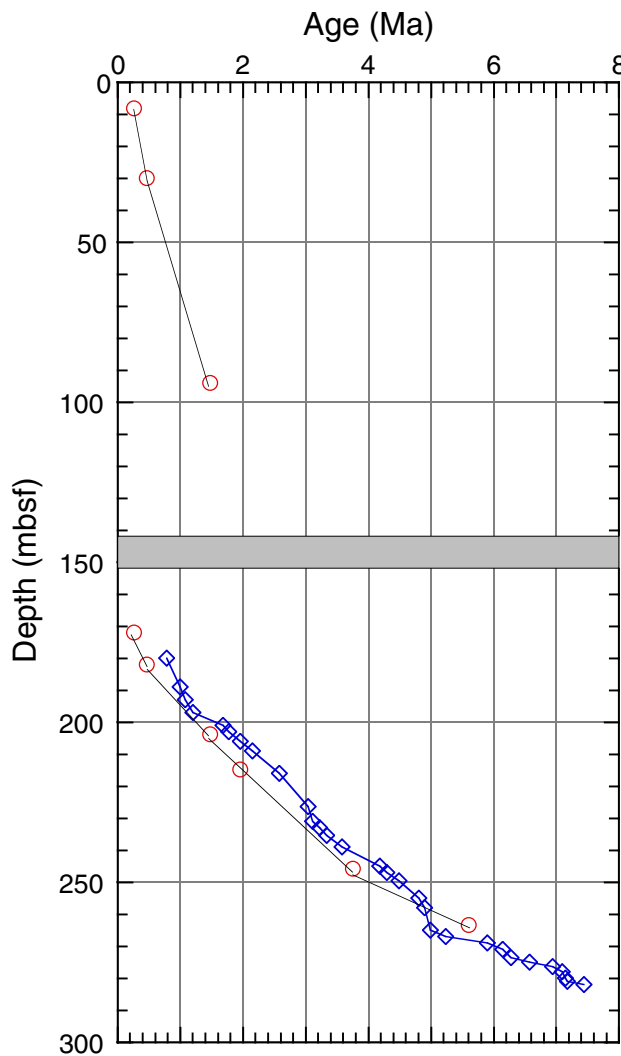


Table T1. Calcareous nannofossil range-distribution chart and nannofossil zonation for Holes 1039A, 1039B, and 1039C. ([See table notes](#). Continued on next nine pages.)

Table T1 (continued).

Table T1 (continued).

Table T1 (continued).

Calcareous nannofossil zone(s)	Core, section, interval (cm)	Depth (mbsf)	
NN19	8H-4, 50-53	64	<i>Discaster hamatus</i>
	8H-6, 50-53	67	<i>Dictyococcites</i> sp.
	8H-CC	68.88	<i>Discaster bolivi</i>
	9H-2, 50-53	70.53	<i>Catinaster mexicanus</i>
	9H-4, 50-53	73.53	<i>Coccoolithus miopelagicus</i>
	9H-6, 50-52	76.53	
	9H-CC	78.37	
	10H-2, 50-53	80	
	10H-4, 50-53	83.03	
	10H-CC	87.98	
	11H-2, 50-53	89.5	
	11H-4, 50-53	92.5	
	11H-6, 50-53	95.5	
	11H-CC	97.37	
	12X-2, 52-54	99.02	
	12X-4, 53-55	102.03	
NN18	12X-6, 50-52	105	
	12X-CC	106.71	
	13X-2, 50-53	105.5	
	13X-4, 122-124	109.22	
	13X-6, 68-70	111.68	
	13X-CC	113.09	
	14X-2, 51-53	115.11	
	14X-4, 52-54	118.12	
	14X-5, 127-129	120.37	
	14X-6, 51-53	121.11	
NN17-NN16	14X-CC	122.7	
	15X-2, 51-53	124.71	
	15X-4, 51-53	127.72	
	15X-6, 51-53	130.72	
	15X-CC	132.42	
NN15-NN13	16X-2, 51-53	134.21	
	16X-4, 50-53	137.2	
	16X-6, 51-54	140.21	
	16X-CC	141.77	
NN12	17X-2, 50-53	143.8	
	17X-4, 50-53	146.8	
	17X-6, 50-53	149.8	
			<i>Discaster deflandrei</i>
			<i>Discaster kugleri</i>
			<i>Discaster signus</i>
			<i>Helicosphaera</i> sp. (small vertical bar)
			<i>Helicosphaera wilcoxini</i>
			<i>Coronocyclus nitescens</i>
			<i>Helicosphaera rhombica</i>
			<i>Cyclargolithus floridanus</i>
			<i>Hayaster perplexus</i>
			<i>Discaster aulakos</i>
			<i>Discaster druggi</i>
			<i>Discaster moorei</i>
			<i>Sphenolithus heteromorphus</i>
			<i>Helicosphaera ampliaperta</i>
			Unidentifiable 6-rayed discasters
			Unidentifiable placooliths
			F
			F
			F
			F

Table T1 (continued).

Table T1 (continued).

Table T1 (continued).

Table T1 (continued).

Calcareous nannofossil zone(s)	Core, section, interval (cm)	Depth (mbsf)	<i>Discaster hamatus</i>	<i>Dictyococcites</i> sp.	<i>Discaster bolivi</i>	<i>Catinaster mexicanus</i>	<i>Coccolithus miopelagicus</i>	<i>Discaster musicus</i>	<i>Discaster deflandrei</i>	<i>Discaster kugleri</i>	<i>Discaster signus</i>	<i>Helicosphaera</i> sp. (small vertical bar)	<i>Helicosphaera wilcoxini</i>	<i>Coronocyclus nitescens</i>	<i>Helicosphaera rhombica</i>	<i>Cyclcocolithus floridanus</i>	<i>Hayaster perplexus</i>	<i>Discaster aulakos</i>	<i>Discaster drugii</i>	<i>Discaster moorei</i>	<i>Sphenolithus heteromorphus</i>	<i>Helicosphaera ampliaperta</i>	Unidentifiable 6-rayed discasters	Unidentifiable placoliths
NN6	26X-CC	238	A															F	F	F	F	F	F	
	27X-2, 48-50	239.98	A	A														R	R	F	F	F	F	
	27X-4, 50-52	243	A															C	C	F	F	F	F	
	27X-6, 51-53	246.01	A															C	C	F	F	F	F	
	27X-CC	247.56	A															F	F	F	F	F	F	
	28X-2, 50-53	249.7	A															R	R	F	F	F	F	
	28X-4, 50-53	252.7	A															C	C	F	F	F	F	
	28X-6, 51-53	255.71	A															C	C	F	F	F	F	
	28X-CC	257.27	A															F	F	F	F	F	F	
	29X-2, 50-53	259.4	A															R	R	F	F	F	F	
	29X-4, 50-53	262.4	A															C	C	F	F	F	F	
	29X-6, 50-53	265.4	A															C	C	F	F	F	F	
	29X-CC	266.84	A															F	F	F	F	F	F	
	30X-1, 125-128	268.35	A															R	R	F	F	F	F	
	30X-3, 125-128	271.35	A															C	C	A	A	A	A	
	30X-5, 50-53	273.6	A															C	C	A	A	A	A	
	30X-CC	274.15	A															F	F	F	F	F	F	
	31X-2, 50-53	278.7	A															R	R	F	F	F	F	
	31X-4, 50-53	281.7	A															C	C	A	A	A	A	
	31X-6, 50-53	284.7	A															C	C	A	A	A	A	
	31X-CC	286.25	A															F	F	F	F	F	F	
	32X-2, 51-53	288.41	A															R	R	F	F	F	F	
	32X-4, 51-53	291.41	A															C	C	A	A	A	A	
	32X-6, 50-52	294.4	F															C	C	A	A	A	A	
	32X-CC	296.14	A															F	F	F	F	F	F	
	33X-2, 52-54	298.02	A															C	C	C	C	C	C	
	33X-4, 51-53	301.01	V															F	F	F	F	F	F	
	33X-6, 50-53	304	A															C	C	C	C	C	C	
	33X-CC	305.67	A															F	F	F	F	F	F	
	34X-2, 50-52	307.6	A															R	R	F	F	F	F	
	34X-4, 53-55	310.63	V															C	C	A	A	A	A	
	34X-6, 52-54	313.62	V															F	F	F	F	F	F	
	34X-CC	315.36	A															R	R	F	F	F	F	
	35X-2, 51-53	317.21	A															C	C	A	A	A	A	
	35X-4, 51-53	320.21	A															F	F	F	F	F	F	
	35X-6, 55-56	323.25	A															C	C	A	A	A	A	
	35X-CC	324.86	A															F	F	F	F	F	F	
NN4	36X-2, 53-55	326.83	A														C	C	A	A	A	F		

Table T1 (continued).

Notes: Abundance: H = highly abundant; V = very abundant; A = abundant; C = common; F = few; R = rare; r = rare reworked; B = barren. Preservation: P = poor; M = moderate; G = good.

Table T1 (continued).

Calcareous nannofossil zone(s)	Core, section, interval (cm)	Depth (mbsf)	<i>Discocaster hamatus</i>	<i>Dictyococcites</i> sp.	<i>Discocaster bolivi</i>	<i>Catinaster mexicanus</i>	<i>Coccolithus miopelagicus</i>	<i>Discocaster musicus</i>	<i>Discocaster deflandrei</i>	<i>Discocaster kugleri</i>	<i>Discocaster signus</i>	<i>Helicosphaera</i> sp. (small vertical bar)	<i>Helicosphaera wilcoxini</i>	<i>Coronocyclus nitescens</i>	<i>Helicosphaera rhombica</i>	<i>Cyclargolithus floridanus</i>	<i>Hayaster perplexus</i>	<i>Discocaster aulakos</i>	<i>Discocaster drugii</i>	<i>Discocaster moorei</i>	<i>Sphenolithus heteromorphus</i>	<i>Helicosphaera ampliaperta</i>	Unidentifiable 6-rayed discocasters	Unidentifiable placooliths
NN4	36X-4, 53-55	329.83	A															F	F	F	F	F		
	36X-6, 53-55	332.83	A	A														A	F	A	F	F		
	36X-CC	334.62	A															A	A	C	C	C		
	37X-2, 53-55	336.43	A															C	C	C	C	C		
	37X-4, 51-53	339.41	A															C	C	C	C	C		
	37X-6, 52-54	342.42	A															C	C	C	C	C		
	37X-CC	344.23	A															C	C	C	C	C		
	38X-2, 50-53	346	A															R	F	A	C	F		
	38X-4, 53-56	349.03	A															F	F	C	F	F		
	38X-6, 50-53	352	C															F	F	A	C	F		
	38X-CC	353.85	A															F	F	A	C	F		
	39X-2, 49-52	355.59	A															R	F	A	C	F		
	39X-4, 49-52	358.59	A															F	F	C	F	F		
	39X-6, 50-53	361.6	A															F	F	A	C	R		
	39X-CC	363.32																F	F	C	A	F		
	40X-2, 58-60	365.28	A															R	F	A	C	F		
	40X-4, 50-53	368.2	C															F	F	A	C	F		
	40X-6, 45-47	371.15	C															R	F	A	C	R		
	40X-CC	372.89	C															F	F	C	A	F		
	41X-1, 115-128	373.95	A															R	F	A	C	C		
	41X-3, 114-116	376.94	A															F	F	A	C	C		
	170-1039C-1R-1, 49-51	363.59	A															R	A	C	C	C		
	1R-3, 48-50	366.45	A															F	F	A	C	A		
	2R-1, 48-50	373.18	A															R	F	A	C	C		
	2R-3, 50-52	375.43	C															F	F	A	C	C		
	3R-1, 50-52	382.8	C															F	F	A	C	C		
	3R-3, 50-53	385.63	C															F	F	A	C	C		
	4R-1, 120-122	393.1	C															F	F	A	C	C		
	5R-1, 51-52	402.01	C															F	F	A	C	C		
	6R-2, 50-52	413.2	A															F	F	A	F	F		
	6R-4, 50-52	416.2	C															F	F	A	F	F		
	7R-2, 25-28	422.05																F	F	A	F	F		

Table T2. Calcareous nannofossil range-distribution chart and nannofossil zonation for Hole 1040B.
(See table notes. Continued on next page.)

Table T2 (continued).

Notes: Abundance: H = highly abundant; V = very abundant; A = abundant; C = common; F = few; f = few reworked; R = rare; r = rare reworked; B = barren. Preservation: P = poor; M = moderate; G = good.

Table T3. Calcareous nannofossil range-distribution chart and nannofossil zonation for Hole 1040C. (See table notes. Continued on next four pages.)

CALCAREOUS NANNOFOSSIL BIOSTRATIGRAPHY

Table T3 (continued).

CALCAREOUS NANOFOSIL BIOSTRATIGRAPHY

Table T3 (continued).

Table T3 (continued).

Table T3 (continued).

Calcareous nannofossil zone(s)	Core, section, interval (cm)	Depth (mbsf)	Abundance	Preservation	<i>Discoaster brouwerii</i>	<i>Reticulofenestra minuta</i>	<i>Helicosphaera carteri</i>	<i>Helicosphaera sellii</i>	<i>Calcidiscus leptoporus</i>	<i>Coccolithus pelagicus</i>	<i>Gephyrocapsa oceanica</i>	<i>Gephyrocapsa caribbeanica</i>	<i>Discoaster pentaradiatus</i>	<i>Gephyrocapsa sinuosa</i>	<i>Pseudomiliaria lacunosa</i>	<i>Gephyrocapsa aperta</i>	<i>Ceratolithus cristatus</i>	<i>Calcidiscus macintyreii</i>	<i>Pontosphaera multipora</i>	<i>Coccolithus miopelagicus</i>	<i>Discoaster intercalans</i>	<i>Reticulofenestra pseudounbilicus</i>	<i>Sphenolithus abies/neobabies</i>	<i>Pontosphaera discopora</i>	<i>Helicosphaera wallichii</i>	<i>Sphenolithus verensis</i>	<i>Ceratolithus rugosus</i>	<i>Discoaster surculus</i>	<i>Discoaster variabilis</i>	<i>Discoaster asymmetricus</i>	<i>Discoaster breggrenii</i>	<i>Triquetrohabdulus farnsworthii</i>	<i>Dictyocites</i> spp.	<i>Discoaster deflandrei</i>	<i>Discoaster exilis</i>	<i>Helicosphaera burkei</i>	<i>Discoaster signus</i>	<i>Coronocyclus nitescens</i>	<i>Cyclicargolithus floridanus</i>	<i>Discoaster kugleri</i>	<i>Sphenolithus heteromorphus</i>	<i>Discoaster moorei</i>	<i>Helicosphaera ampli/aperita</i>	unidentifiable 6-rayed discoaster	unidentifiable placoliths
NN5	46R-2, 50-52	594.3	V	M	A C		F A																																						
	46R-4, 50-52	597.3	V	A	A C		F A																																						
	46R-CC	598.86	A	M	C C		F																																						
	47R-2, 50-52	603.9	A	M	A C		C																																						
	47R-4, 50-52	606.9	A	M	A C		C																																						
	47R-6, 50-52	609.9	V	M	A C		A																																						
	47R-CC	611.78	A	M	C F		F																																						
	48R-2, 50-52	613.6	V	M	A		A																																						
	48R-4, 50-52	616.6	V	M	A		A																																						
	48R-6, 50-52	619.6	V	M	A		F A																																						
	48R-CC	621.45	A	M	C		R C																																						
NN4	49R-2, 50-52	623.2	V	M	C		F C																																						
	49R-4, 50-52	626.2	V	M	C		F C																																						
	49R-6, 50-52	629.2	V	M	C		F A																																						
	50R-2, 50-52	632.8	V	M	A		C A																																						
	50R-4, 52-54	635.82	A	M	A		F C																																						
	50R-6	638.28	A	M	C		F																																						
	51R-2, 50-52	642.4	A	M	A		F C																																						
	51R-4, 54-56	645.34	B																																										
	51R-CC	646.55	A	P	C		F																																						
	52R-1, 125-128	651.25	A	P																																									
	52R-3, 32-34	653.32	B																																										

Notes: Abundance: H = highly abundant; V = very abundant; A = abundant; C = common; F = few; R = rare; r = rare reworked; B = barren. Preservation: P = poor; M = moderate; G = good.

Table T4. Calcareous nannofossil range-distribution chart and nannofossil zonation for Holes 1041A, 1041B, and 1041C. ([See table notes](#). Continued on next four pages.)

Table T4 (continued).

Table T4 (continued).

Table T4 (continued).

Table T4 (continued).

Calcareous nannofossil zone(s)	Core, section, interval (cm)	Depth (mbsf)	Abundance	Preservation	small reticulofenestrids	<i>Emiliania huxleyi</i>	<i>Gephyrocapsa oceanica</i>	<i>Pontosphaera discopora</i>	<i>Pseudoemiliania lacunosa</i>	<i>Discoaster brauwei</i>	<i>Calcidiscus leptoporus</i>	<i>Helicosphaera carteri</i>	<i>Heicosphaera wallichi</i>	<i>Pontosphaera</i> spp.	<i>Coccilithus pelagicus</i>	<i>Helicosphaera sellii</i>	<i>Ceratolithus cristatus</i>	<i>Discoaster pentaradiatus</i>	<i>Discoaster surculus</i>	<i>Reticulofenestra pseudoumbilicus</i>	<i>Sphenolithus abies</i>	<i>Sphenolithus verensis</i>	<i>Ceratolithus rugosus</i>	<i>Ceratolithus armatus</i>	<i>Discoaster asymmetricus</i>	<i>Discoaster quinqueramus</i>	<i>Discoaster pergrenii</i>	<i>Coccilithus miopelagicus</i>	<i>Cyclargolithus floridanus</i>	<i>Discoaster deflandrei</i>	<i>Discoaster neorectus</i>	<i>Hayaster perplexus</i>	<i>Calcidiscus macintyrei</i>	<i>Discoaster intercalaris</i>	<i>Discoaster variabilis</i>	<i>Discoaster lugleri</i>	<i>Sphenolithus heteromorphus</i>	<i>Helicosphaera ampliaperta</i>	<i>Discoaster challengerii</i>	<i>Coronoclylus nitescens</i>	Unidentifiable placoliths	Unidentifiable 6-ray discoasters
Older than NN11	1R-CC	397.61	R	P		<i>Emiliania huxleyi</i>																																				
	2R-1, 50-52	405.2	B				<i>Gephyrocapsa oceanica</i>																																			
	2R-2, 125-127	406.85	B					<i>Pontosphaera discopora</i>																																		
	2R-CC	407.51	F	P	F																																					
	3R-1, 12-15	414.32	B	P	C																																					
	3R-CC	415.54	A	P																																						
Cruciplacolithus primus (early to late Paleocene) observed in Core 170-1041A-4X-CC																																										
Micula murus (Maastrichtian) observed in Core 170-1041B-19R-CC.																																										

Notes: Abundance: H = highly abundant; V = very abundant; A = abundant; C = common; F = few; R = rare; r = rare reworked; B = barren. Preservation: P = poor; M = moderate; G = good.

Table T5. Calcareous nannofossil range-distribution chart and nannofossil zonation for Holes 1042A and 1042B.

Calcareous nannofossil zone(s)	Core, section, interval (cm)	Depth (mbsf)	Abundance	Preservation	Small reticulofenestrids	<i>Calcaisicus epitoporus</i>	<i>Coccinithus micpeagicus</i>	<i>Cyclicangolithus iliondanus</i>	<i>Discoaster quinqueramus</i>	<i>Helicosphaera caerula</i>	<i>Sphenolithus heteromorphus</i>	<i>Sphenolithus moniformis</i>	<i>Sphenolithus verensis</i>	<i>Discoaster brouwei</i>	<i>Discoaster variabilis</i>	<i>Helicosphaera sellii</i>	<i>Reticulofenestra pseudumbilicus</i>	<i>Coccinithus pelagicus</i>	<i>Gephyrocapsa caribbeana</i>	<i>Coccinithus pelagicus</i>	<i>Calcaisicus macintyrei</i>	<i>Discoaster berggreni</i>	<i>Discoaster dellandrei</i>	<i>Helicosphaera ampliaperta</i>
Unable to delineate zones because of sparse nannofossils and lack of stratigraphic continuity	170-1042A-1R-CC	49.93	F	P	F	F				R														
	2R-CC	97.73	R	P	R	R																		
	3R-CC	156.26	F	P	F	F				R														
	4R-CC	203.92	B	B																				
	5R-CC	212.88	R	P	R	R				R														
	6R-CC	223.18	R	P	R	R				R	R	R	R	R	R	R	R	R	R	R	R	R	R	
	7R-CC	231.65	R	P	R	R				R	R	R	R	R	R	R	R	R	R	R	R	R	R	
	170-1042B-3R-CC	333.26	A	M	F	A	A	A	A	A	A	A	A	C			A	R			C	A		
	5R-CC	354.72	F	P	F					F			F	F										
	6R-CC	363.14	R	P					R			R	R	R					R	R				
	8R-CC	383.47	F	P					F	F	F	F	F	A			F							

Notes: Abundance: H = highly abundant; V = very abundant; A = abundant; C = common; F = few; R = rare; B = barren. Preservation: P = poor; M = moderate; G = good.

Table T6. Calcareous nannofossil range-distribution chart and nannofossil zonation for Hole 1043A. ([See table notes](#). Continued on next two pages.)

Table T6 (continued).

J.P. MUZA
CALCAREOUS NANNOFOSSIL BIOSTRATIGRAPHY

59

Table T6 (continued).

Calcareous nannofossil zone(s)	Core, section, interval (cm)	Depth (mbfs)	Abundance	Preservation	<i>Emiliania huxleyi</i>	<i>Gephyrocapsa caribbeanica</i>	<i>Gephyrocapsa oceanica</i>	<i>Helicosphaera carteri</i>	<i>Helicosphaera sellii</i>	<i>Calcidiscus leptoporus</i>	<i>Coccilithus pelagicus</i>	<i>Calcidiscus macintyrei</i>	<i>Pseudoemiliania lacunosa</i>	<i>Coronocyclus nitescens</i>	<i>Pontosphaera discospora</i>	<i>Helicosphaera neogranulata/ryalina</i>	<i>Reticulofenestra pseudumbilicus</i>	<i>Sphenolithus abies/neodobies</i>	<i>Sphenolithus moriformis</i>	<i>Pontosphaera verensis</i>	<i>Helicosphaera wallachii</i>	<i>Reticulofenestra asanoi</i>	<i>Cyclocalathus floridanus</i>	<i>Coccilithus micipelagicus</i>	<i>Discoaster dellandrei</i>	<i>Discoaster intercalans</i>	<i>Helicosphaera ampliaperta</i>	<i>Sphenolithus heteromorphus</i>	<i>Discoaster brouweri</i>	<i>Ceratolithus rugosus</i>	<i>Pontosphaera multipora</i>	<i>Triquetorhabdulus rugosus</i>	<i>Umbilicosphaera mirabilis</i>	<i>Catinaster mexicanus</i>	<i>Ceratolithus cristatus</i>	<i>Discoaster calcans</i>	<i>Discoaster variabilis</i>	<i>Discoaster pentaradiatus</i>	<i>Ceratolithus acutus</i>	<i>Discoaster asymmetricus</i>	<i>Discoaster pseudovariabilis</i>	<i>Discoaster surculus</i>	<i>Discoaster triradiatus</i>	<i>Discoaster quinqueramus/berggreni</i>	<i>Helicosphaera burkei</i>	<i>Catinaster altos</i>	<i>Discoaster neocrinus</i>	<i>Discoaster tamalis</i>	<i>Discoaster bellus</i>	<i>Discoaster intercalaris</i>	<i>Discoaster prepentaradiatus</i>	<i>Discoaster nemamatetus</i>	<i>Discoaster sanguinolensis</i>	<i>Sphaerolithus spissus</i>	<i>Mallomonas spissula</i>	<i>Unidentified polygonal</i>	<i>Pontosphaera sp.</i>	D. aff. <i>surculus</i>	Unidentified 6-rayed
NN19	24X-2, 50-52	216.8	B																																																								
	24X-4, 50-53	219.8	B																																																								
	24X-6, 50-53	222.8	B																																																								
	24X-CC	224.53	A M	F F F F A	r	F				F																																																	
	25X-2, 50-52	226.5	A	F M	A F C A	C F	C			F R																																																	
	25X-4, 50-53	229.5	F	M	F F	F R	F			F C R F																																																	
NN18–NN16	25X-6, 50-53	232.5	C M	F F	F F	F C R F																																																					
	25X-CC	234.33	F P	F P	F F	F C R F																																																					
	26X-2, 50-52	236.1	F	P																																																							
	26X-4, 50-53	239.1																																																									
NN15–NN12	26X-CC	241.91	C M		C	C R			F		F F		A F F																																														
	27X-2, 47-49	245.67	A G		A	C			F		C A		A A F																																														
	27X-4, 50-52	248.7	B		A	A			F		A A		A A																																														
	27X-6, 48-50	251.68	A M		A F	A F			F		F F F		F F F																																														
	27X-CC	253.55	C M		F	C			F		A C		A C																																														
	28X-2, 50-52	255.3	A M		F	V G			C		A A F		V V		A C																																												
	28X-4, 50-52	258.3	V G		C	F C			F		A V		V C																																														
	28X-6, 50-52	261.3	V G		C	F			F		C F F																																																
	28X-CC	263.13	C G																																																								
	29X-2, 50-52	265	A M																																																								
	29X-4, 50-52	268	V G		C																																																						
NN11	29X-6, 50-52	271	V G	F F	F	A A	C		F		V A F		A																																														
	29X-CC	272.84	C G																																																								
	30X-2, 50-52	274.6	V G	C F	F F	C A	A																																																				
	30X-4, 50-52	277.6	A M																																																								
	30X-6, 50-52	280.6	A M																																																								
	30X-7, 5-47	281.65	C M			F	C C			A F F			F	R	C																																												
	30X-CC	282.26	C M		C C F						A F F																																																

Notes: Abundance: H = highly abundant; V = very abundant; A = abundant; C = common; F = few; f = few reworked; R = rare; r = rare reworked; B = barren. Preservation: P = poor; M = moderate; G = good.

Table T7. Age assignments to bottom and top of the observed ranges of calcareous nannofossil species.

Index Fossil	Nannofossil datums	Age (Ma)
<i>Emiliania huxleyi</i>	B	0.26
<i>Psuedoemiliania lacunosa</i>	T	0.46
<i>Helicosphaera sellii</i>	T	1.47
<i>Discoaster brouwerii</i>	T	1.95
<i>Discoaster pentaradiatus</i>	T	2.55
<i>Reticulofenestra pseudoumbilicus</i>	T	3.75
<i>Sphenolithus abies/neoabies</i>	T	3.75
<i>Triquetrorhabdulus rugosus</i>	T	5.34
<i>Discoaster quinqueramus</i>	T	5.6
<i>Discoaster loeblichii</i>	T	7.4
<i>Discoaster berggrenii</i>	B	8.6
<i>Discoaster loeblichii</i>	B	8.7
<i>Discoaster hamatus</i>	T	9.4
<i>Discoaster hamatus</i>	B	10.7
<i>Coccolithus miopelagicus</i>	T	10.8
<i>Discoaster kugleri</i>	T	11.5
<i>Discoaster kugleri</i>	B	11.8
<i>Cyclicargolithus floridanus</i>	T	11.8
<i>Sphenolithus heteromorphus</i>	T	13.6
<i>Helicosphaera ampliaperta</i>	T	15.6
<i>Sphenolithus heteromorphus</i>	B	18.2

Notes: B = bottom; T = top. Datums and ages are from Berggren et al. (1995a, 1995b).

Table T8. Definition of calcareous nannofossil zonation scheme of Martini (1971) and Bukry (1973b, 1975) and Okada and Bukry (1980).

Calcareous nannofossil zone definition	Calcareous nannofossil zone	
	Martini (1971)	Bukry (1973b, 1975); Okada and Bukry (1980)
FO <i>Emiliania huxleyi</i> to Recent	NN21	CN15
LO <i>Pseudoemiliania lacunosa</i> to FO <i>Emiliania huxleyi</i>	NN20	CN14b
FO <i>Gephyrocapsa oceanica</i> to FO <i>Gephyrocapsa caribbeanica</i>		CN13b
LO <i>Discoaster brouwerii</i> to FO <i>G. caribbeanica</i>		CN13a
LO <i>Discoaster brouwerii</i> to LO <i>P. lacunosa</i>	NN19	
LO <i>Discoaster pentaradiatus</i> to LO <i>D. brouwerii</i>	NN18	CN12d
LO <i>Discoaster surculus</i> to LO <i>D. pentaradiatus</i>	NN17	CN12c
LO <i>Discoaster tamalis</i> to LO <i>D. surculus</i>		CN12b
LO <i>Reticulofenestra pseudoumbilica</i> to LO <i>D. tamalis</i>		CN12a
LO <i>Reticulofenestra pseudoumbilica</i> to LO <i>D. surculus</i>	NN16	
FO <i>Discoaster asymmetricus</i> acme to LO <i>R. pseudoumbilica</i>	NN15	CN11b
FO <i>Discoaster asymmetricus</i> to LO <i>A. tricornulatus/Amaurolith</i> extinction		NN14
LO <i>Amaurolithus primus</i> to FO <i>D. asymmetricus</i> acme		CN11a
FO <i>Ceratolithus rugosus</i> to FO <i>D. asymmetricus</i>	NN13	
FO <i>C. rugosus</i> to LO <i>A. primus</i>		CN10c
LO <i>Trigetrarhabdus rugosus</i> or FO <i>C. acutus</i> to FO <i>C. rugosus</i> or LO <i>C. acutus</i>		CN10b
LO <i>Discoaster quinqueramus</i> to LO <i>T. rugosus</i> or FO <i>C. acutus</i>		CN10a
LO <i>Discoaster quinqueramus</i> to FO <i>C. rugosus</i> and/or LO <i>C. acutus</i>		NN12
FO to LO of <i>Discoaster quinqueramus</i>	NN11	
FO <i>D. berggrenii</i> and/or FO <i>D. surculus</i> to LO <i>D. quinqueramus</i>	NN10	CN9
LO <i>Discoaster hamatus</i> to FO <i>D. quinqueramus</i>		
FO <i>D. berggrenii</i> to FO <i>D. surculus</i>		CN8
FO <i>Discoaster neorectus</i> to FO <i>D. berggrenii</i>		CN8b
LO <i>D. hamatus</i> to FO <i>D. neorectus</i>		CN8a
FO to LO <i>D. hamatus</i>	NN9	CN7a+b
FO <i>Catinaster coalitus</i> to FO <i>D. hamatus</i>	NN8	CN6
FO <i>Discoaster kugleri</i> or <i>C. floridanus</i> to FO <i>C. coalitus</i>	NN7	CN5b
LO <i>Sphenolithus heteromorphus</i> to FO <i>D. kugleri</i> or LO <i>C. floridanus</i>	NN6	CN5a
FO <i>Helicosphaera ampliaperta</i> to LO <i>S. heteromorphus</i>	NN5	CN4
LO <i>Sphenolithus belemnos</i> to LO <i>H. ampliaperta</i>	NN4	CN3

Note: FO = first occurrence; LO = last occurrence.

Table T9. Nannofossil zone assigned to depth observed in apron sediments from Site 1041.

Depth (mbsf)	Age (calcareous nannoplankton zonal range)
0-2	N21-NN19
2-13.9	NN21-NN17
13.9-134.25	NN18-NN17
134.25-275.21	NN16-NN11
275.21-415.54	older than NN11

Note: Zonation is from Martini (1971).

Table T10. Composite summary of the Pleistocene, Pliocene, and late and middle Miocene calcareous nannofossil datums identified in cored sequences along with their ages and depth locations within the cores.

Index fossil	Nannofossil datums		Depth of top and/or bottom (mbsf)				
	Top/ Bottom	Age (Ma)	Site 1039	Site 1040 underthrust	Site 1041	Site 1043 prism	Site 1043 underthrust
<i>Emiliania huxleyi</i>	B	0.26	31.03			7.99	171.8
<i>Pseudoemiliania lacunosa</i>	T	0.46	48.75	405.74		29.76	181.89
<i>Helicosphaera sellii</i>	T	1.47	97.3	417.37		1.47	203.6
<i>Discoaster brouwerii</i>	T	1.95	105.5	449.8			214.47
<i>Discoaster pentaradiatus</i>	T	2.55	120.37	462.4			
<i>Reticulofenestra pseudoumbilicus</i>	T	3.75	134.21	472.75			245.67
<i>Sphenolithus abies/neoabies</i>	T	3.75	134.21	472.75			245.67
<i>Triquetrorhabdulus rugosus</i>	T	5.34	149.8				
<i>Discoaster quinqueramus</i>	T	5.6	151.9	477.99			263.13
<i>Discoaster loeblichii</i>	T	7.4	166.11				
<i>Discoaster berggrenii</i>	B	8.6	168.35	483.46			
<i>Discoaster loeblichii</i>	B	8.7	170.73				
<i>Discoaster hamatus</i>	T	9.4	175.63				
<i>Discoaster hamatus</i>	B	10.7	180.37				
<i>Coccolithus miopelagicus</i>	T	10.8	182.21	501			
<i>Discoaster kugleri</i>	T	11.5	189.87	510.48			
<i>Discoaster kugleri</i>	B	11.8	198.65	516.54			
<i>Cyclicargolithus floridanus</i>	T	11.8	201.51				
<i>Sphenolithus heteromorphus</i>	T	13.6	259.4	553.94			
<i>Helicosphaera ampliaperta</i>	T	15.6	326.83	629.2			
<i>Sphenolithus heteromorphus</i>	B	18.2					

Unable to determine